FINNISH METEOROLOGICAL INSTITUTE
CONTRIBUTIONS

No. 92

MULTI-SPACECRAFT STUDIES ON SPACE PLASMA SHOCKS

Heli Hietala

Department of Physics
Faculty of Science
University of Helsinki
Helsinki, Finland

Academic dissertation in theoretical physics

To be presented, with the permission of the Faculty of Science of the University of Helsinki, for public criticism in the small auditorium E204 of Physicum at Kumpula Campus (Gustaf Hällströmin katu 2a) at 12 o'clock noon on 21st September, 2012.

Finnish Meteorological Institute
Helsinki, 2012

ISBN 978-951-697-769-3 (paperback)
ISBN 978-951-697-770-9 (PDF)
ISSN 0782-6117
Unigrafia
Helsinki, 2012

FINNISH METEOROLOGICAL INSTITUTE

Published by Finnish Meteorological Institute
(Erik Palménin aukio 1) , P.O. Box 503
FIN-00101 Helsinki, Finland

Series title, number and report code of publication
Contributions 92, FMI-CONT-92

Date August 2012

Author(s)

Heli Hietala

Name of project

Commissioned by

Title

Multi-Spacecraft Studies on Space Plasma Shocks

Abstract

Just like in liquids and gases, there are shock waves in the space plasma environment of our planet. As the high speed plasma flow of the solar wind hits the magnetosphere of the Earth, a bow shock is formed. Disturbances propagating in the solar wind flow, such as massive eruptions of Sun's plasma and magnetic field, can also drive shock waves ahead of them. These integral parts of our natural plasma environment are, despite being ubiquitous, a poorly understood physical phenomenon. Furthermore, shocks are components of space weather phenomena that can have severe socio-economical impacts such as hampering the operation of telecommunication systems and satellite navigation.

In this dissertation we use simultaneous observations from several spacecraft as well as numerical simulations to address certain open questions in plasma shock physics. The thesis consists of four scientific articles and an introductory part that presents the findings within the context of the field. The theoretical foundations of collisionless shock physics are briefly reviewed and the employed methods (data-analysis, modelling, and numerical simulations) are described. The previous observational studies of space plasma shocks as well as relevant simulation work are discussed. The main focus is on the dynamic structure of shocks and the phenomena in their vicinity that arise from this.

The first two articles address particle acceleration in shock-shock interaction - a fundamental acceleration mechanism that often takes place in astrophysical environments but that is very rarely seen with direct observations. We perform a detailed analysis of a shock-shock interaction event with the best spacecraft coverage reported so far. The novel result is the first *in situ* observations of the particle release at shock collision, further verified with a simulation study.

In the third article we investigate a class of transient phenomena in the magnetosheath region between the bow shock and the magnetosphere of the Earth: Earthward directed jets with a high speed unexpected for the subsolar region. Based on the detailed multi-spacecraft observations we propose a formation mechanism for the jets whose source had remained unexplained. We infer a connection between the rippling of shock fronts evident in many observations and simulations and the structuring of the downstream region. In the fourth article we analyse a set of jets and show that the proposed mechanism based on the bow shock ripples can account for their main properties, including their finite spatial scale and the observed range of dynamic pressure. Furthermore, we investigate the possible role of these high dynamic pressure jets in the solar wind-magnetosphere interaction. We find that their effects can be seen in the magnetosphere all the way to the ground magnetometers.

Publishing unit
Earth Observation

Classification (UDC)

52, 533.9

Keywords
space plasma physics, shock waves, acceleration of particles

ISSN and series title
0782-6117 Finnish Meteorological Institute Contributions

ISBN
978-951-697-769-3 (paperback), 978-951-697-770-9 (PDF)

Language
English

Pages
130

ILMATIETEEN LAITOS

Julkaisun sarja, numero ja raporttikoodi
Contributions 92, FMI-CONT-92

Julkaisija Ilmatieteen laitos, (Erik Palménin aukio 1)
PL 503, 00101 Helsinki

Julkaisuaika elokuu 2012

Tekijä(t)

Heli Hietala

Projektin nimi

Toimeksiantaja

Nimeke

Tutkimuksia avaruusplasmojen shokki-ilmiöistä monisatelliittihavainnoin

Tiivistelmä

Kuten nesteissä ja kaasuissa, myös planeettaamme ympäröivässä plasmassa voi edetä shokkiaaltoja. Kun Auringosta lähtevä jatkuva varattujen hiukkasten virta, aurinkotuuli, osuu Maan magnetosfääriin niiden väliin muodostuu keulashokki. Vastaavasti aurinkotuulessa etenevät häiriöt kuten Auringon koronan massiiviset purkaukset voivat ajaa shokkiaaltoja edellään. Yleisyydestään huolimatta nämä luonnollisen plasmaympäristömme osaset ovat huonosti ymmärretty fysiikan ilmiö. Shokit ovat myös tärkeässä roolissa niissä avaruussääilmiöissä, joilla voi olla vakavia sosioekonomisia seurauksia. Esimerkiksi lähiavaruuden shokkien tuottamat korkeaenergiaiset hiukkaset muodostavat erityisen suuren riskin astronauteille ja satelliittien herkälle elektroniikalle.

Tässä väitöskirjassa tarkastellaan avaruusplasmashokkien fysiikkaa käyttäen useiden satelliittien samanaikaisia havaintoja sekä mallinnusta. Väitöskirja koostuu neljästä vertaisarvioidusta tieteellisestä artikkelista ja johdanto-osasta, jossa artikkelien tulokset esitetään avaruusfysiikan tutkimusalan kontekstissa. Törmäyksettömien shokkien fysiikan teoreettinen perusta sekä tutkimuksessa käytetyt menetelmät (data-analyysi, mallinnus ja numeeriset simulaatiot) kerrataan lyhyesti. Lisäksi esitellään shokkihavaintoja käsitteleviä tutkimuksia ja niihin liittyviä simulaatioita pääpainon ollessa shokkien dynaamisessa rakenteessa sekä muuttuvan geometrian seurauksena shokkien ympäristössä esiintyvissä ilmiöissä.

Väitöskirjan ensimmäisessä ja toisessa artikkelissa tutkitaan hiukkasten kiihdytystä kahden shokin vuorovaikutuksessa. Shokkienvälisiä törmäyksiä tapahtuu usein ja monissa eri plasmaympäristöissä, mutta niihin liittyvistä prosesseista on hyvin vaikea saada suoria havaintoja. Ensimmäisessä artikkelissa analysoidaan tarkasti törmäys, jossa poikkeuksellisen kattavat satelliittihavainnot mahdollistavat eri prosessien yksityiskohtaisen tarkastelun. Tutkimuksen päätulos ovat ensimmäiset *in situ* -havainnot hiukkasten vapautumisesta shokkien törmätessä. Väitöskirjan toisessa artikkelissa tämä tulkinta varmistetaan simulaatioin.

Kahdessa jälkimmäisessä tutkimuksessa tarkastellaan Maan magnetosfäärin ja keulashokin välisen magnetosheath-alueen erittäin nopeita, paikallisia virtauksia. Tämän tyyppisiä poikkeuksellisia virtauksia on havaittu jo aiemmin, mutta niiden syntymekanismia ei ole tunnettu. Väitöskirjan kolmannessa artikkelissa esitetään yksityiskohtaisten satelliittihavaintojen pohjalta, että virtaukset aiheutuvat keulashokin paikallisesta aaltoilusta. Neljännessä artikkelissa analysoidaan usean tällaisen virtauspurskeen ominaisuuksia ja osoitetaan niiden olevan yhteensopivia esitetyn syntymekanismin kanssa. Lopuksi tarkastellaan, miten nopeiden virtausten suuri dynaaminen paine kytkee ne osaksi Maan magnetosfäärin ja ionosfäärin laajempaa dynamiikkaa.

Julkaisijayksikkö
Uudet havaintomenetelmät

Luokitus (UDK)

52, 533.9

Asiasanat
avaruusplasmafysiikka, shokkiaallot, hiukkaskiihdytys

ISSN ja avainnimike
0782-6117 Finnish Meteorological Institute Contributions

ISBN
978-951-697-769-3 (paperback), 978-951-697-770-9 (PDF)

Kieli
englanti

Sivumäärä
130

Contents

Preface

The work leading to this thesis was carried out in the Department of Physics, University of Helsinki. The Finnish Graduate School in Astronomy and Space Physics, the Väisälä foundation, and the Academy of Finland are thanked for financial support. Funding from the Magnus Ehrnrooth Foundation and the Emil Aaltonen Foundation in the form of travel grants is also gratefully acknowledged.

First and foremost, my gratitude goes to my supervisors. I want to thank Prof. Hannu Koskinen for taking me into his group and supporting me in my enterprises throughout my doctoral studies. He pointed me towards the field of spacecraft observations and data analysis. Likewise, I want to thank Doc. Rami Vainio for our long discussions on topics ranging from physics and life in the academia to life in general. He has been a demanding mentor and an inspiring example. I have enjoyed working with you both during these years.

I thank my co-authors, colleagues, and friends at the University of Helsinki and the Finnish Meteorological Institute, in Finland and abroad. In particular, I want to thank Dr. Neus Agueda, Dr. Katerina Andréeová, Dr. Emilia Kilpua, Dr. Tiera Laitinen, Dr. Noora Partamies, Jens Pomoell and Dr. Arto Sandroos for your guidance, encouragement and companionship.

Last but not least, I wish to thank my family for their support and Tuomas, my boyfriend, for taking care of me.

Heli Hietala
London, August 2012

Acronyms and Abbreviations

3DP	Three-Dimensional Plasma and energetic particle investigation (onboard Wind spacecraft)
ACE	Advanced Composition Explorer
AE	Auroral Electrojet index
AU	Astronomical Unit
AXIOM	Advanced X-ray Imaging Of the Magnetosphere
C1–C4	the four Cluster spacecraft
CANMOS	Canadian Magnetometer Observatory Network
CARISMA	Canadian Array for Realtime Investigations of Magnetic Activity
CIR	Co-rotating Interaction Region
CIS	Cluster Ion Spectrometry experiment (onboard Cluster spacecraft)
CME	Coronal Mass Ejection
CDAWeb	Coordinated Data Analysis Web
DARTS	Data ARchives and Transmission System
dHT	de Hoffmann–Teller frame
DOK	Detektor Ochlazdajemyj Kremnijevyj—passively cooled silicon detector (onboard Interball spacecraft)
EPAM	Electron, Proton, and Alpha Monitor (onboard ACE spacecraft)
EPIC	Energetic Particles and Ion Composition instrument (onboard Geotail spacecraft)
ESA	European Space Agency
FGM	FluxGate Magnetometer instrument (onboard Cluster spacecraft)
FS	Forward Shock
FTE	Flux Transfer Event
GOES	Geostationary Operational Environmental Satellite
GPS	Global Positioning System

GSE	Geocentric Solar Ecliptic coordinate system
GSFC	Goddard Space Flight Center
HIA	Hot Ion Analyser (part of CIS)
IBEX	Interstellar Boundary EXplorer
ICME	Interplanetary Coronal Mass Ejection
ICS	Ion Composition Subsystem (part of EPIC)
IMF	Interplanetary Magnetic Field
IMP	Interplanetary Monitoring Platform
IP	InterPlanetary
JAXA	Japan Aerospace Exploration Agency
L1	first Lagrangian point
LASCO	Large Angle and Spectrometric Coronagraph (onboard SOHO spacecraft)
LEMS	Low Energy Magnetic Spectrogram (part of EPAM)
MIE	Magnetic Impulse Event
MGF	Magnetic Field Experiment (onboard Geotail spacecraft)
MHD	MagnetoHydroDynamics
MLT	Magnetic Local Time
MVA	Minimum Variance Analysis
NASA	National Aeronautics and Space Administration
NSSDC	National Space Science Data Center
PIC	Particle-In-Cell
RD	Rotational Discontinuity
RS	Reverse Shock
SC	SpaceCraft
SIR	Stream Interaction Region
SLAMS	Short Large Amplitude Magnetic Structure
SOHO	SOlar and Heliospheric Observatory
SPDF	Space Physics Data Facility
SST	Solid State Telescope (part of 3DP)
STEREO	Solar TErrestrial RElations Observatory
SuperDARN	Super Dual Auroral Radar Network
SW	Solar Wind
SWE	Solar Wind Experiment (onboard Wind spacecraft)
SWEPAM	Solar Wind Electron, Proton and Alpha Monitor (onboard ACE spacecraft)
TCV	Travelling Convection Vortex
TD	Tangential Discontinuity
THEMIS	Time History of Events and Macroscale Interactions during Substorms
ULF	Ultra Low Frequency

UT	Universal Time
VDP	Vsjenapravlenyj Datcik Plazmy—omnidirectional plasma detector (onboard Interball spacecraft)

Publications

This thesis consists of an introductory part and four articles. The introduction contains background for the studies and the main results reached in the articles. The original abstracts of the articles are given below. The contribution of the author of this dissertation to the articles is summarised at the end.

Paper I

Hietala, H., Agueda, N., Andréeová, K., Vainio, R., Nylund, S., Kilpua, E. K. J., and Koskinen, H. E. J., "In situ observations of particle acceleration in shock-shock interaction", *Journal of Geophysical Research*, **116**, A10105, 2011.

Abstract: We use detailed multispacecraft observations to study the interaction of an interplanetary (IP) shock with the bow shock of the Earth on August 9–10, 1998. We can distinguish four different phases of particle acceleration in the shock-shock interaction: (1) formation of magnetic contact with IP shock and the seed population of energetic particles accelerated by it, (2) reacceleration of this population by the bow shock, (3) first order Fermi acceleration as the two shocks approach each other, and (4) particle acceleration and release as the shocks collide. Such a detailed analysis was made possible by the particularly advantageous quasi-radial interplanetary magnetic field configuration. To our knowledge this is the first time the last phase of acceleration at a shock-shock collision has been reported using in situ space plasma observations.

Paper II

Hietala, H., Sandroos, A., and Vainio, R., "Particle Acceleration in Shock–Shock Interaction: Model to Data Comparison", *The Astrophysical Journal Letters*, **751**, L14, 2012.

Abstract:

Shock–shock interaction is a well-established particle acceleration mechanism in astrophysical and space plasmas, but difficult to study observationally. Recently, the interplanetary shock collision with the bow shock of the Earth on 1998 August 10 was identified as one of the rare events where detailed in situ observations of the different acceleration phases can be made. Due to the advantageous spacecraft and magnetic field configurations, in 2011, Hietala et al. were able to distinguish the seed population and its reacceleration at the bow shock, as well as the Fermi acceleration of particles trapped between the shocks. They also interpreted their results as being the first in situ evidence of the release of particles from the trap as the two shocks collided. In the present study we use a global 2.5D test-particle simulation to further study particle acceleration in this event.We concentrate on the last phases of the shock–shock interaction, when the shocks approach and pass through each other. The simulation results verify that the main features of the measurements can be explained by shock–shock interaction in this magnetic geometry, and are in agreement with the previous interpretation of particle release. Shock–shock collisions of this type occur commonly in many astrophysical locations such as stellar coronae, planetary and cometary bow shocks, and the distant heliosphere.

Paper III

Hietala, H., Laitinen, T. V., Andréeová, K., Vainio, R., Vaivads, A., Palmroth, M., Pulkkinen, T. I., Koskinen, H. E. J., Lucek, E. A., and Rème, H., "Supermagnetosonic Jets behind a Collisionless Quasiparallel Shock", *Physical Review Letters*, **103**, 45001, 2009.

Abstract: The downstream region of a collisionless quasiparallel shock is structured containing bulk flows with high kinetic energy density from a previously unidentified source. We present Cluster multispacecraft measurements of this type of supermagnetosonic jet as well as of a weak secondary shock front within the sheath, that allow us to propose the following generation mechanism for the jets: The local curvature variations inherent to quasiparallel shocks can create fast, deflected jets accompanied by density variations in the downstream region. If the speed of the jet is super(magneto)sonic in the reference frame of the obstacle, a second shock front forms in the sheath closer to the obstacle. Our results can be applied to collisionless quasiparallel shocks in many plasma environments.

Paper IV

Hietala, H., Partamies, N., Laitinen, T. V., Clausen, L. B. N., Facskó, G., Vaivads, A., Koskinen, H. E. J., Dandouras, I., Rème, H., and Lucek, E. A.,"Supermagnetosonic subsolar magnetosheath jets and their effects: from the solar wind to the ionospheric convection", *Annales Geophysicae*, **30**, 33–48, 2012.

Abstract: It has recently been proposed that ripples inherent to the bow shock during radial interplanetary magnetic field (IMF) may produce local high speed flows in the magnetosheath. These jets can have a dynamic pressure much larger than the dynamic pressure of the solar wind. On 17 March 2007, several jets of this type were observed by the Cluster spacecraft. We study in detail these jets and their effects on the magnetopause, the magnetosphere, and the ionospheric convection. We find that (1) the jets could have a scale size of up to a few R_{E} but less than $\sim 6\,R_{\mathrm{E}}$ transverse to the X_{GSE} axis; (2) the jets caused significant local magnetopause perturbations due to their high dynamic pressure; (3) during the period when the jets were observed, irregular pulsations at the geostationary orbit and localised flow enhancements in the ionosphere were detected. We suggest that these inner magnetospheric phenomena were caused by the magnetosheath jets.

Author's contribution

The topics of all papers were decided with the co-authors. In **Paper I** the author was responsible for the data-analysis, constructed the semi-empirical models for the interpretation, and wrote the manuscript. In **Paper II** the author participated in the application of the numerical model to the observed event, carried out the comparison of simulated and observed data, and wrote the manuscript with the help of the co-authors. In **Paper III** the author led the interpretation of the data and the conceptualisation of the proposed mechanism, performed the main parts of the data analysis, and wrote the manuscript. In **Paper IV** the author carried out the main parts of the data analysis and interpretation, and wrote the manuscript with the assistance of the co-authors.

Chapter 1

Introduction

We live our everyday lives surrounded by neutral fluids, such as air and water, flowing at subsonic speeds. Outside the protection of the atmosphere and magnetic field of our planet, however, most of the matter in the universe is in ionised state—plasma—and often moving at supersonic speeds. For the study of the complex phenomena in that medium, the near-Earth space is the best laboratory we have.

The study of our natural plasma environment that can be probed with *in situ* measurements is called space physics. The physical and phenomenological state of that environment is described by *space weather* [e.g., Watermann et al., 2009]. The emphasis is often put on the threatening aspects of space weather due to their socio-economical relevance. Indeed the time-varying electromagnetic and particle conditions can hamper the operation of technological systems in space or on ground, such as communication satellites and the Global Positioning System (GPS). Changes in space weather can also be dangerous for human health, e.g, for astronauts working outside the space station. One of the objectives of space physics is to understand the processes in the near-Earth space well enough to forecast space weather, so that it would be possible to prepare for strong disturbances—*space storms*.

On the other hand plasma physics is basic research towards understanding of the fundamental physical processes in our environment. The inherent nonlinearity of plasma physics makes analytical studies difficult. The coupled spatial, temporal and energy scales pose challenges also for numerical approach, and the current computing power is sufficient only in relatively simple cases. There are and have been several scientific spacecraft to gather plenty of observational data, but not enough to form a network with a good coverage of the whole near-Earth space. Often a fruitful approach to space physics research questions is to combine theoretical knowledge, analysis of

observational data, and numerical experiments to reach better understanding of the complex phenomena.

One of the core research topics of space physics is the continuous stream of charged particles flowing out from the Sun—the *solar wind*. The solar wind carries with itself the magnetic field of the Sun so that it permeates the heliosphere as an *interplanetary magnetic field* (IMF). The solar wind with its magnetic field is the driver of the dynamics of Earth's *magnetosphere*, i.e., the region dominated by the magnetic field of our planet.

Just like in liquids and gases, there are *shock waves* in plasmas. For example when the solar wind hits the magnetosphere of the Earth, a *bow shock* is formed. *Interplanetary shocks* propagate in the solar wind, often driven by *coronal mass ejections* (CMEs)—massive eruptions of Sun's plasma and magnetic field. Despite being ubiquitous, shock waves in space plasmas are a poorly understood physical phenomenon. They are nonlinear, irreversible, and cause significant changes in the properties of the medium they propagate in. Furthermore, plasma shocks accelerate charged particles to very high energies. The *energetic particles* produced by the Solar System space plasma shocks pose a particular threat to both astronauts and spacecraft electronics.

The scientific objective of this thesis is to combine multi-point observations, modelling, and numerical simulations to address certain open questions related to shock physics. Specifically,

- we perform a detailed analysis of one of the rare shock–shock interaction events suitable for an *in situ* study;
- we consider the formation of fast flows donstream of the Earth's bow shock whose source has remained unexplained.

These two studies, while aiming for better physical understanding of space plasma shocks, have connections to astrophysics and laboratory plasma physics as well. They are also part of the research on transient phenomena in solar wind–magnetosphere interaction that constitute space weather.

The thesis is organised as follows. The theoretical background and the employed methods are described in Chapter 2. Chapter 3 introduces the observational studies related to the themes of this thesis—the dynamic geometry of shocks and the related phenomena in their vicinity. Chapter 4 presents the results of the four articles with further analysis and discussion. The first two articles address particle acceleration in shock–shock interaction. The third proposes a mechanism for high speed jets observed downstream of supercritical shocks, and the fourth analyses such jets in the magnetosheath as well as their effects on the magnetosphere. Conclusions and outlook are given in Chapter 5.

Chapter 2

Theory and Methodology

This chapter briefly presents the theoretical foundations of plasma shock physics as well as the main methods used in Chapters 3 and 4.

2.1 Plasma

Plasma is quasi-neutral gas containing enough free charges to make collective electromagnetic interactions significant for its behaviour. Furthermore, the space plasmas considered in this thesis are called collisionless, meaning that they are so hot and dilute that the collisional mean free paths are large compared to the spatial scale of the system under consideration. Hence binary collisions between particles are rendered unimportant compared to the collective electromagnetic interactions. To a degree, one can thus envision the electromagnetic fields binding the plasma elements together and giving it properties similar to ordinary fluids. On the other hand, it is these collective phenomena that pose challenges to the theoretical description of plasmas.

There are several levels of theory for plasmas depending on the physical problem of interest. Three primary levels (illustrated in Figure 2.1) are the following [e.g., Choudhuri, 1998; Koskinen, 2011]: The motion of a single plasma particle can be treated using classical electrodynamics and Maxwell's equations. Kinetic description of the time-evolution of collisionless plasma using distribution functions is called the Vlasov theory. The continuum descriptions of plasma as one or more fluids are numerous. The limit of simplification, i.e., the treatment of plasma as a single fluid with infinite conductivity is referred to as ideal magnetohydrodynamics (MHD). The main topic of this thesis, shock waves, is an example where the different scales are tightly coupled to each other. Hence the study of their physics requires maneuvering between different levels of description.

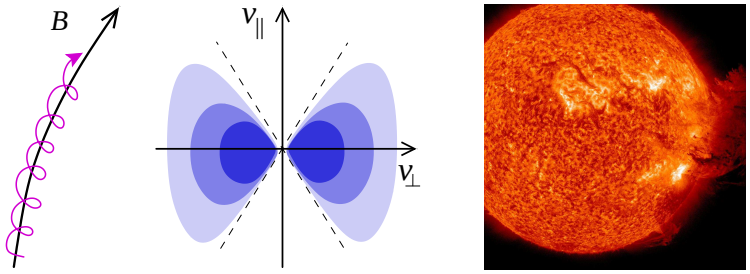

Figure 2.1: Left: the motion of a charged particle (magenta) along a magnetic field line (black). Centre: an example of a plasma distribution function in velocity space. Right: Plasma falling down to solar surface after a CME as captured by NASA's Solar Dynamics Observatory.

2.2 Shocks

When a finite-size obstacle moves in a fluid medium the fluid needs information of the incoming object to be able to flow around it. In neutral fluids this information is mediated by sound waves. The *sound speed* V_S of a fluid is given by $\sqrt{\gamma k_B T/m}$, where γ is the polytropic index, k_B the Boltzmann constant, T the temperature and m the mean mass of the fluid particles. The relevant dimensionless quantity to characterise the flow is the ratio of the velocity of the flow to the sound speed: the (sonic) Mach number M_S.

If the object moves at a supersonic speed, i.e., faster than the information can be transferred in the medium, the fluid has no knowledge of the incoming object. Nature's solution to this problem is the formation of a shock wave—a discontinuity ahead of the object where part of the kinetic energy of the incoming flow is transformed into heat. Thus in the region between the obstacle and the shock wave the velocity of the medium relative to the object drops below the local sound speed and the fluid can flow around the obstacle.

In a plasma, there are numerous wave modes that can carry the information. Considering plasma in the MHD picture, the possibilities are limited to three wave modes and three characteristic speeds [e.g., Koskinen, 2011]. In addition to the sound speed, there is the *Alfvén speed* $V_\mathrm{A} = \sqrt{B^2/\mu_0\rho_m}$, where B is the magnitude of the ambient magnetic field, ρ_m the mass density of the plasma and μ_0 the permeability of vacuum. The (compressional) fast and slow MHD waves have phase velocities that are combinations of these two:

$$V_{\mathrm{f}}^2 = \frac{1}{2}(V_\mathrm{S}^2 + V_\mathrm{A}^2) \mp \frac{1}{2}\sqrt{(V_\mathrm{S}^2 + V_\mathrm{A}^2)^2 - 4V_\mathrm{S}^2 V_\mathrm{A}^2 \cos^2\theta}, \qquad (2.1)$$

where the indices s and f correspond to the solutions with the minus and plus signs, and θ is the angle between the ambient magnetic field $\mathbf{B}$ and the wave vector $\mathbf{k}$. The shear (intermediate) Alfvén waves propagate at the phase velocity of $V_\mathrm{A}\cos\theta$. The third and the highest characteristic speed, called the *magnetosonic speed* $V_\mathrm{MS} = \sqrt{V_\mathrm{S}^2 + V_\mathrm{A}^2}$, is the velocity of the fast wave propagating perpendicular to the magnetic field ($\theta = \pi/2$).

The relevant Mach number for the shock formation is the ratio between the component of plasma velocity parallel to the shock wave vector (shock normal) evaluated in the reference frame moving with the shock and the phase velocity of the wave mode in the plasma frame. The fast-wave Mach number calculated in this manner was considered, e.g., in **Paper IV**. Often in practice, however, one simply considers the Alfvén Mach number and the magnetosonic Mach number.

Heating of the downstream fluid requires dissipation inside the shock front. In neutral fluids this is achieved via collisions and consequently the thickness of the shock front is of the order of the collisional mean free path. In collisionless plasmas the process must be different, as the observed space plasma shocks are much thinner than the mean free paths, but what are the mechanisms at play? When faced with this problem the picture of electromagnetic fields bringing about fluid-like properties is again instructive. More precisely, the self-consistent back-reaction between the particles and the fields is essential. As conventional resistivity is inadequate in highly conductive space plasmas, anomalous resistivity due to wave–particle interactions is often invoked to account for the dissipation. The reflection of a part of the incoming ion population also plays an important role at higher Mach numbers. For a more detailed presentation on the various heating mechanisms the reader is referred to Kennel et al. [1985] and Krauss-Varban [2010]. Although the 'shock problem' was stated decades ago, the details of the nonlinear processes involved are still not well understood.

Collisionless shocks are indeed very difficult to describe from the first principles, but fortunately there are plenty of observational data as shocks are ubiquitous in space. As the solar wind is supermagnetosonic, magnetised planets as well as planets with an atmosphere have a *bow shock* in front of them (Figure 2.2(a)). Naturally, the most detailed and extensive data on collisionless shocks are from the bow shock of the Earth. Its geometry and observed features will be described in detail in Section 3.1.

The interplanetary (IP) shocks encountered in the solar wind have two types of origin. CMEs travelling in the interplanetary space—*interplanetary coronal mass ejections* (ICMEs)—that are fast enough can drive a bow shock ahead of them (Figure 2.2(b)). These are the most common IP

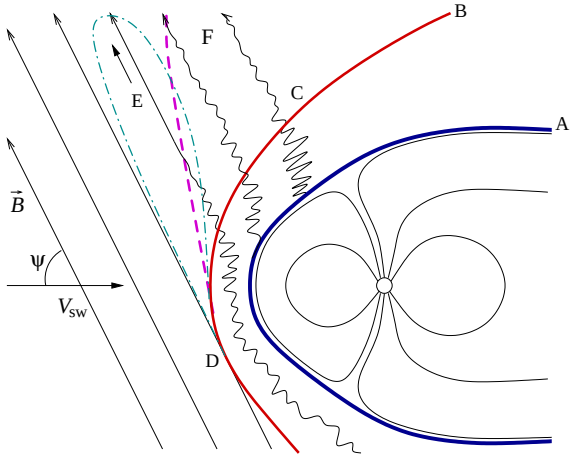

(a) Bow shock of the Earth. The different regions indicated by the letters A–F are described in detail in Section 3.1

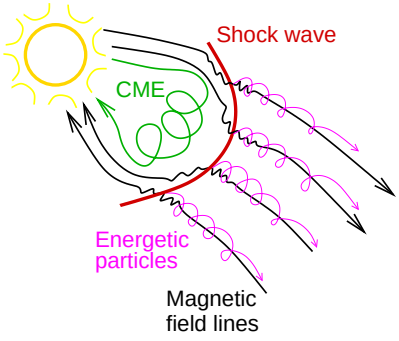

(b) CME-driven shock.

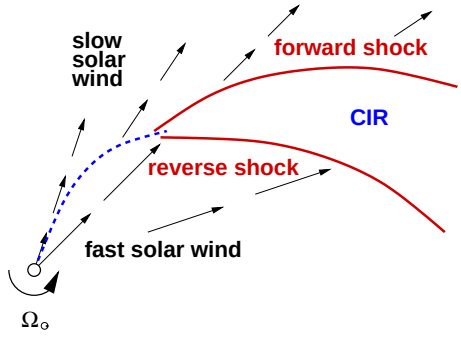

(c) CIR-related shock pair.

Figure 2.2: Examples of space plasma shocks.

shocks at 1 AU, especially during the solar maximum [Oh et al., 2007]. The second type are formed due to the inhomogeneity of the solar wind outflow: As the Sun rotates, compression regions are produced where the fast solar wind flowing out from equator-ward extensions of the polar coronal holes catches up with the slow wind emitted earlier from the equatorial streamer belt. Inside Earth orbit, these stream interaction regions (SIRs) are bounded by forward and reverse waves propagating along and against the solar wind flow, respectively. At large heliospheric distances SIRs strengthen and the two waves steepen into a pair of forward and reverse shocks separated by a *co-rotating interaction region* (CIR), as illustrated in Figure 2.2(c). The steepening into shocks can take place already between Venus at 0.72 AU and the Earth [Russell et al., 2009], but typically beyond 1 AU [Hundhausen and Gosling, 1976].

Close to the Sun, *coronal shocks* can be driven by solar flares in addition to CMEs. At the outer edge of the heliosphere, the super(magneto)sonic solar wind must slow down to interface with the magnetised interstellar plasma. Voyager I and II spacecraft crossed the *heliospheric termination shock* in 2004 and 2007 [Fisk, 2005; Jokipii, 2008] and stirred the space physics community with new, puzzling observations. There may also exist an additional bow shock if the heliosphere moves at a super(magneto)sonic speed with respect to the interstellar medium. Astrophysical shocks such as supernova shocks, though fascinating, are beyond the scope of this work.

The nature of the shock transition in a space plasma depends strongly on the shock obliquity, that is, on the angle θ_{Bn} between the upstream magnetic field and the nominal shock normal [Stone and Tsurutani, 1985]. The rudimentary explanation for this difference is illustrated in Figure 2.3. When θ_{Bn} is large, i.e., the shock is *quasi-perpendicular*, particles reflected

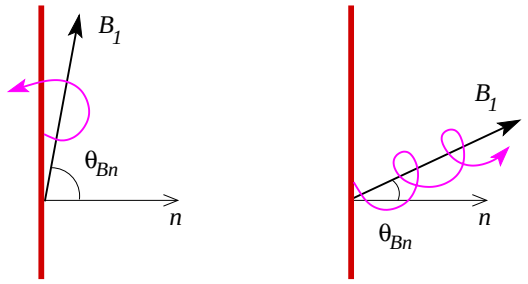

Figure 2.3: Motion of a charged particle (magenta) near a shock front (red). The reflected particles gyrate back into a quasi-perpendicular shock (left), while they escape from a quasi-parallel shock (right).

from the shock will gyrate back into it. In contrast when the shock is *quasi-parallel*, the reflected particles can escape upstream and interact with the incident plasma over long distances.

In the next two subsections, we will briefly present the description of shocks as discontinuities (2.2.1), and how they accelerate particles depending on their obliquity (2.2.2). Yet the real shocks observed in space, be they planetary or interplanetary, are not infinitely large, planar structures with smooth upstream conditions. The spatial and temporal changes in the shock geometry, as well as the diversity of phenomena emerging from these changes in the shock surroundings, are the theme of this thesis and shall be discussed in more detail in the following Chapters.

2.2.1 MHD description

The description of shock waves within the framework of MHD can be found in most plasma physics textbooks [e.g., Boyd and Sanderson, 2003; Koskinen, 2011]. This subsection highlights the steps relevant for the discussion in the rest of this thesis.

Let us consider a planar discontinuity in the fluid properties that has an infinitesimal thickness and a normal vector $\mathbf{n}$. Working in the frame of reference moving with the discontinuity, let us further assume time stationarity ($\partial_t = 0$) and that the only variations are along the discontinuity normal. With these assumptions the problem becomes essentially one-dimensional and the ideal MHD equations (the conservation of mass, momentum, and energy together with the divergence-free condition for the magnetic field) can be integrated to get jump conditions of the form $0 = \{\mathbf{F}(0^+) - \mathbf{F}(0^-)\} \cdot \mathbf{n} \equiv \mathbf{F}_2 \cdot \mathbf{n} - \mathbf{F}_1 \cdot \mathbf{n} \equiv [\mathbf{F} \cdot \mathbf{n}]$. Here 1 and 2 stand for values of the quantity $\mathbf{F}$ upstream and downstream of the discontinuity. The induction equation can be manipulated into a similar form to complete the set of equations. The result is known as the MHD Rankine-Hugoniot relations:

$$[\rho_m V_\mathrm{n}] = 0 \tag{2.2}$$

$$[\rho_m V_\mathrm{n}^2 + P + \frac{B_\mathrm{t}^2}{2\mu_0}] = 0 \tag{2.3}$$

$$[\rho_m \mathbf{V}_\mathrm{t} V_\mathrm{n} - \frac{\mathbf{B}_\mathrm{t} B_\mathrm{n}}{\mu_0}] = 0 \tag{2.4}$$

$$[\frac{1}{2}\rho_m V^2 V_\mathrm{n} + \frac{\gamma P}{\gamma - 1} V_\mathrm{n} + \frac{B_\mathrm{t}^2}{\mu_0} V_\mathrm{n} - \frac{\mathbf{V}_\mathrm{t} \cdot \mathbf{B}_\mathrm{t}}{\mu_0} B_\mathrm{n}] = 0 \tag{2.5}$$

$$[B_\mathrm{n}] = 0 \tag{2.6}$$

$$[\mathbf{V}_\mathrm{t} B_\mathrm{n} - \mathbf{B}_\mathrm{t} V_\mathrm{n}] = 0. \tag{2.7}$$

Here the indices n and t refer to the vector components normal and tangential to the discontinuity, and $\mathbf{V}$ is the velocity and P the thermal pressure of the plasma.

In order to be a shock wave, the discontinuity has to be both compressive and have a finite mass flux across it. The special cases of exactly perpendicular and parallel shocks will not be considered here, as the great majority of real shocks are oblique. Let us first consider the most convenient frame for the analysis, as there exist an infinite number of rest frames for a planar shock. For oblique shocks the relevant one is called the de Hoffmann–Teller (dHT) frame. This frame moves along the shock surface at a speed such that the upstream magnetic field is aligned with the upstream plasma flow, and consequently the upstream convective electric field vanishes. This also holds on the downstream side, and thus energy is conserved in the dHT frame. The transformation velocity is given by

$$\mathbf{v}_{\mathrm{dHT}} = \frac{\mathbf{n} \times (\mathbf{V}_1 \times \mathbf{B}_1)}{\mathbf{n} \cdot \mathbf{B}_1}, \tag{2.8}$$

so that the upstream velocity becomes $\dfrac{V_{1\mathrm{n}}}{\cos\theta_{Bn}}\hat{\mathbf{b}}$, where $\hat{\mathbf{b}}$ is the unit vector in the direction of the magnetic field.

In the de Hoffmann–Teller frame, the jump conditions for oblique shocks can be written as

$$\frac{\rho_{m2}}{\rho_{m1}} = r \tag{2.9}$$

$$\frac{V_{2\mathrm{n}}}{V_{1\mathrm{n}}} = \frac{1}{r} \tag{2.10}$$

$$\frac{V_{2\mathrm{t}}}{V_{1\mathrm{t}}} = \frac{M_{\mathrm{A1}}^2 - 1}{M_{\mathrm{A1}}^2 - r} \tag{2.11}$$

$$\frac{B_{2\mathrm{n}}}{B_{1\mathrm{n}}} = 1 \tag{2.12}$$

$$\frac{B_{2\mathrm{t}}}{B_{1\mathrm{t}}} = r\frac{M_{\mathrm{A1}}^2 - 1}{M_{\mathrm{A1}}^2 - r} \tag{2.13}$$

$$\frac{P_2}{P_1} = r + \frac{(\gamma - 1) r V_1^2}{2 V_{\mathrm{S1}}}\left(1 - \frac{V_2^2}{V_1^2}\right), \tag{2.14}$$

where r is the shock compression ratio, $M_{\mathrm{A1}} = V_{1\mathrm{n}}\sqrt{\mu_0 \rho_{m1}}/B_{1\mathrm{n}}$ the upstream Alfvén Mach number and V_{S1} the upstream sound speed.

There are three types of shock solutions to the jump conditions:

fast For fast shocks the upstream velocity along the shocks normal is super-fast-magnetosonic $V_{1\mathrm{n}} > V_{\mathrm{f1}}$, while in the downstream region

$V_{2n} < V_{f2}$. The tangential magnetic field increases across the fast shock $B_{2t} > B_{1t}$. The vast majority of shocks observed in space plasmas are of the fast type.

slow Similarly to fast shocks, upstream of slow shocks the flow is super-slow-magnetosonic $V_{1n} > V_{s1}$, while in the downstream region $V_{2n} < V_{s2}$. The tangential magnetic field decreases across the shock front $B_{2t} < B_{1t}$, but retains its sign. Slow shocks are an integral part of the models for magnetic reconnection.

intermediate The third type of shock solutions exists for $1 < M_{A1}^2 < r$, $r > 1$, and is called the intermediate wave. The tangential magnetic field changes its sign at the discontinuity. These waves are non-evolutionary, i.e., unstable against disintegrating into more than one discontinuity. Thus they are in fact unphysical solutions, at least as freely propagating plasma shocks.

The Rankine-Hugoniot relations (2.3–2.7) have also other, non-shock type of discontinuities as their solutions. In **Paper I**, we refer to a tangential discontinuity (TD), where there is no plasma flow across the discontinuity and only the total pressure remains unchanged. The notable feature of TDs is that the plasma populations on each side are not magnetically connected to each other. When discussing the studies related to **Paper III** and **Paper IV**, we encounter also rotational discontinuities (RDs), where there is a finite flow across the discontinuity, but no compression. The magnetic field magnitude stays constant and the tangential component changes sign in the non-trivial case.

2.2.2 Mechanisms for particle acceleration

The proton energy distribution in the solar wind consists of a quasi-Maxwellian thermal core around 1 keV plus a time-varying power law tail of suprathermals and higher energy particles extending many orders of magnitude [e.g., Giacalone, 2010]. The energetic particles in the 100 keV/nucleon–100 MeV/nucleon range can be further classified as 'steady-state' or quiet time background and transient enhancements associated with CIR- and CME-related shocks and solar eruptive events. (Anomalous and galactic cosmic rays are not discussed here.) The ubiquitous presence of these energetic populations in the vast heliosphere is understandable as the plasma is collisionless.

According to the current knowledge, the two main phenomena accelerating the energetic particles are shock waves and magnetic reconnection; although shock waves are an important part of reconnection models as well,

as noted in the previous subsection. The basics of shock acceleration are well described in textbooks and reviews, see, e.g., Krauss-Varban [2010] and the references therein. Here we only note the main principles.

Shock Drift Acceleration (SDA) is a family of processes where a part of the particle distribution gains energy through drifting in the convective electric field $\mathbf{E} = -\mathbf{V} \times \mathbf{B}$ of the shock. At the shock magnetic field jump, the gradient and curvature drifts displace the particles in opposite directions with respect to the electric field, the former increasing the particles' energy and the latter decreasing it. For quasi-perpendicular shocks, the gradient drift wins for most particles.

Alternatively, for oblique shocks, we can consider SDA by transforming into the de Hoffmann–Teller frame. Since the electric field in this frame is zero, the energy as well as the magnetic moment of the particle are conserved. Depending on its pitch-angle, a particle can reflect from the shock's magnetic field increase. Upon subsequent transformation back to the upstream rest frame one finds that the energy of the reflected particle has increased.

The energy gains in SDA are very limited, typically less than a factor of ten. Thus the question is how to make the particles cross the shock multiple times. The answer probably lies in turbulence.

Fermi [1949] proposed the following mechanism for the generation of cosmic rays: charged particles propagating in interstellar space will frequently collide with moving, large scale magnetic irregularities (magnetic mirrors). If there is an equal amount of head-on and tail-on collisions, the particle distribution simply broadens and a small part of the population will reach high energies. If the head-on collisions dominate, there is a net gain in energy. In the special case where a particle gets caught between two regions of high field moving against each other along a magnetic field line, fairly large increases in energy will occur, but the particle's pitch-angle will also decrease. Due to this decrease the particle will eventually pass through one of the high magnetic field mirrors. In **Paper I** and **Paper II** we had the opportunity to analyse particle acceleration in an event where two shocks approached each other in a setup quite similar to this.

A modern version of Fermi's idea is the Diffusive Shock Acceleration (DSA), where the role of the magnetic mirrors is taken by scattering centres—the waves generated by the particles themselves—embedded in the converging flow through a shock. Apart from making the particle cross the shock multiple times (and gain energy through SDA during each crossing), the scattering with the dominant head-on collisions will also contribute to the acceleration. This type of process easily emerges at quasi-parallel shocks,

where the reflected particles streaming against the incoming flow can trigger instabilities and wave growth (Figure 2.3).

2.3 Analysis of spacecraft data

The work described in this thesis is based on *in situ* measurements made with instruments onboard several near-Earth spacecraft. The underlying principle has been to make use of all available observation points and their measurements in order to form a coherent picture of the event and find answers to the plasma physics research questions. This section briefly presents the different spacecraft and the typical set of instruments, as well as how the data were obtained and how the basic shock properties were computed from the data. The numerous acronyms have been gathered to the separate section at the beginning of the thesis.

2.3.1 Instruments and data sets

In **Paper I** and **Paper II** the key measurements came from three spacecraft: ACE [Stone et al., 1998], Wind [Acuña et al., 1995], and Geotail [Nishida, 1994]. Data from Interball-Tail [05] and IMP-8 [06] satellites were used to support the analysis. The studies described in **Paper III** and **Paper IV** were centered around ESA's Cluster mission [Escoubet et al., 1997]. Cluster consists of four identical spacecraft moving in a tetrahedron-like formation with a varying separation. In these studies, ACE and Wind were employed as solar wind monitors, while Geotail provided information of the bow shock location. For the inner-magnetospheric investigation of **Paper IV** we used magnetometer observations from the GOES satellites [Grubb, 1975]. We also utilised SuperDARN [Greenwald et al., 1995; Chisham et al., 2007] radar measurements and ground-based magnetometer data from CARISMA and CANMOS chains.

Apart from the geostationary GOES satellites, all spacecraft used in this thesis are spin-stabilised, i.e., rotating around a given axis. This design is useful for the analysis of vector fields and anisotropic particle distributions. The set of instruments and measured quantities varies from spacecraft to spacecraft. Moreover, the instruments onboard a spacecraft are combined into packages—experiments—with varying composition. The key measurements for the studies of **Paper I**–**Paper IV** came from experiments measuring magnetic fields, thermal ions, and energetic particles. Their main features are presented below. Descriptions of the instruments in auxiliary roles, such as electron, electric field, and waves instruments, can be found in the instrument papers cited in the original publications.

The magnetic field data were obtained from fluxgate magnetometers measuring fluctuations at frequencies up to $\sim 10\,\mathrm{Hz}$. The typical spin-stabilised spacecraft setup consists of two triaxial sensors mounted on one (or two) booms allowing to monitor also the magnetic effects due to the spacecraft itself. The challenge of this setup is the determination of the offset in the field component parallel to the spacecraft spin axis. The calibration is done using inflight data with a procedure depending on the plasma regions the spacecraft encounters. On some spacecraft the fluxgate magnetometers are accompanied by search coil magnetometers (up to $\sim 1\,\mathrm{kHz}$) for measuring fast changes in the field. The details of the Geotail MGF experiment, the fluxgate magnetometers of which have essentially the same design as the magnetic field instruments of Wind and ACE, can be found in Kokubun et al. [1994]. The somewhat newer FGM on Cluster is described in Balogh et al. [2001].

Particle instruments collect the plasma particles for one or more spin periods of the rotating spacecraft in order to measure their fluxes. The distribution function of the thermal particles (around 1 keV for solar wind protons in the spacecraft frame) gives the bulk plasma moments such as the density, velocity, and temperature. The suprathermal population and the energetic tail distribution (around 10 keV and $\gtrsim$100 keV for protons) provide information of the acceleration processes. There is large variety in the design of these instruments; a comprehensive discussion on the different elements and configurations can be found in Gloeckler [2010]. In this thesis, the bulk plasma properties were provided by electrostatic analyser based instruments (SWEPAM on ACE [McComas et al., 1998]; CIS on Cluster [Rème et al., 2001]) and Faraday cup sensors (SWE on Wind [Ogilvie et al., 1995]; VDP on Interball [Safrankova et al., 1997]). The energetic particle data were obtained from solid state detector telescopes (SST, part of the multi-sensor 3DP experiment on Wind [Lin et al., 1995]; LEMS sensors of the EPAM experiment on ACE [Gold et al., 1998]; ICS of the EPIC experiment on Geotail [Williams et al., 1994]; DOK-2 on Interball [05]).

The main body of data used in this thesis was obtained through NASA's GSFC/SPDF Coordinated Data Analysis Web (CDAWeb) interface at NSSDC [03]. Access to Cluster data was provided by ESA's Cluster Active Archive [02]. Geotail high resolution magnetic field data were obtained through DARTS at Institute of Space and Astronautical Science, JAXA in Japan [04]. CARISMA and CANMOS data were downloaded from the Canadian Space Science Data Portal [01]. ACE, Wind, and Geotail energetic particle measurements as well as the SuperDARN data were obtained directly from the co-authors working in the instrument teams.

2.3.2 Analysis methods

After the data acquisition the next task is to calculate the main shock characteristics—the normal vector $\mathbf{n}$ and the speed $V_{\rm sh}$ in the normal direction. Apart from being fundamental to the interpretation of the event, the normal vector and speed estimates for shocks and other discontinuities can serve as building blocks for semi-empirical models [**Paper I**] and numerical simulations [**Paper II**]. As there are several methods with their own caveats, it is worthwhile to compute estimates using different methods and compare the results whenever possible. In this subsection we briefly describe the main methods employed in the thesis, first for the normal and then for the speed. A detailed discussion of the different methods and their implementation can be found, e.g., in Schwartz [1998], while Russell et al. [2000] provides an application and comparison of various techniques using the observations of an IP shock on September 24, 1998.

Magnetic co-planarity is based on the notion that, according to the Rankine-Hugoniot conditions presented in Section 2.2.1, the upstream and downstream magnetic field vectors $\mathbf{B}_1$ and $\mathbf{B}_2$ lie in the same plane with the shock normal. Using this knowledge the normal vector can easily be computed as

$$\mathbf{n} = \pm \frac{(\mathbf{B}_2 \times \mathbf{B}_1) \times (\mathbf{B}_2 - \mathbf{B}_1)}{|(\mathbf{B}_2 \times \mathbf{B}_1) \times (\mathbf{B}_2 - \mathbf{B}_1)|}. \tag{2.15}$$

Clearly the method fails for exactly parallel and perpendicular shocks. On the other hand, magnetic field data are generally available and they are measured at a greater cadence and accuracy than the plasma data, making the method preferable to the velocity co-planarity and mixed mode normals [Schwartz, 1998; Russell et al., 2000].

In theory, the upstream and downstream values should be measured quasi-simultaneously as a particular plasma parcel crosses the shock from one side to the other. Typically this is not possible, and all single spacecraft methods such as magnetic co-planarity assume time stationarity of the shock front. The estimates are usually quite sensitive to the choice of upstream and downstream (average) values. Thus it is recommendable to compare different averaging intervals. The shock transition region itself should be carefully excluded. However, the values should be taken quite close to the shock to mimic simultaneous sampling and to avoid inclusion of other plasma structures.

Minimum Variance Analysis (MVA) [e.g., Sonnerup and Scheibles, 1998] identifies the direction along which the set of (magnetic) field measurements has minimum variance. If a unique direction with a clear minimum eigenvalue is found, it corresponds to the normal direction in the case of shocks

with $B_{2n} = B_{1n}$. The method fails for pure MHD shock solutions for which the minimum variance direction is degenerate. The ratio of the intermediate eigenvalue and the minimum eigenvalue gives an indication of the quality of the normal estimate: the ratio should be large, preferably larger than 10. Another quality test is the sensitivity of the MVA estimate with respect to the choice of analysis interval, as was pointed out with the magnetic co-planarity estimates. Note that, as opposed to the data interval for magnetic co-planarity, the MVA interval must contain the transition layer.

The *four-spacecraft method* [e.g., Russell et al., 1983] can be employed when the same shock front or other discontinuity is observed by several spacecraft like the Cluster quartet. The relative positions of the spacecraft and timing can be used to construct a set of equations of the form

$$\frac{(\mathbf{r}_1 - \mathbf{r}_\alpha) \cdot \mathbf{n}}{V_{\rm sh}^{\rm sc}} = (t_1 - t_\alpha). \tag{2.16}$$

Here $\mathbf{r}_\alpha$ and t_α are the location and the time of the observation at spacecraft α, $\alpha = 2 \ldots 4$, and spacecraft 1 has been taken as reference. $V_{\rm sh}^{\rm sc}$ is the shock speed in the spacecraft frame. Assuming that the discontinuity is a plane moving uniformly across the spacecraft, Equation set (2.16) can be solved for $\mathbf{n}/V_{\rm sh}^{\rm sc}$.

The merit of the four-spacecraft method is that only data for the spacecraft location and for the identification of the discontinuity, such as magnetic field measurements, are needed. However, the consistent identification of the crossing times can be difficult. Moreover, the method gives good results only when the spacecraft are non-co-planar, i.e., when the spacecraft form a good tetrahedron. This is a drawback for near-Earth interplanetary studies as most of the currently active spacecraft lie close to the ecliptic plane.

The second important shock characteristic is the shock speed $V_{\rm sh}$. If a suitable multi-spacecraft configuration is available, then the four-spacecraft method can be used as it gives the shock velocity along with the normal vector. Single-spacecraft shock normal estimates calculated with, e.g., the magnetic co-planarity or MVA can be combined with the Mass Flux Algorithm to obtain the shock speed, provided that accurate plasma observations exist.

The *Mass Flux Algorithm* is based on Equation (2.3) which gives the conservation of mass across the shock front in the frame of reference moving with shock. When rewritten in terms of velocities measured in the spacecraft frame, it can be solved for $V_{\rm sh}^{\rm sc}$ giving

$$V_{\rm sh}^{\rm sc} = \frac{(\rho_{m2}\mathbf{V}_2^{sc} - \rho_{m1}\mathbf{V}_1^{sc}) \cdot \mathbf{n}}{\rho_{m2} - \rho_{m1}}. \tag{2.17}$$

All methods described above assume that the shock front is planar and essentially one-dimensional. The validity of this assumption depends significantly on the type of the shock and the scale under consideration, as will be shown in Section 3.1 where observations of shock geometry are discussed in detail.

2.4 Numerical simulations

Numerical modelling is an indispensable tool for increasing our understanding of plasma shock physics. Simulations are also frequently vital companions to observations when trying to decipher what is going on at the shock. Depending on the scientific question and computing power at hand, space plasma shocks have been studied using such approaches as

MHD The MHD fluid equations are solved numerically, typically in a conservative form. MHD simulations are used for large scale studies, such as CME lift-off [Pomoell et al., 2008], CME–CME interactions [Lugaz et al., 2008], and the heliospheric termination shock location [Washimi et al., 2007]. Many phenomena related to, e.g., particles reflected from quasi-parallel shocks are not resolved in this single fluid picture.

Hybrid In quasi-neutral hybrid simulations the ions are treated as (macro-)particles while the electrons form a neutralising fluid. As this approach allows the simulation of counter-streaming ion populations in quite large domains, it has recently been heavily exploited to study the various phenomena around the quasi-parallel bow shock [e.g., Lin and Wang, 2005; Omidi et al., 2005; Blanco-Cano et al., 2009]. The shortcomings of this approach are that the set of equations, though self-consistent, cannot be formulated in a conservative form, and that there is a significant amount of noise stemming from the 'granular' treatment of ions.

Particle-In-Cell In PIC simulations both ions and electrons are represented by computational, finite size particles. The fields and forces generated by these macro-particles are solved on a grid. This type of models have been used to study the microphysics of shocks, e.g., the non-stationarity of the shock front [Lembège et al., 2009], microinstabilities [Umeda et al., 2012] and radio emission from shocks [Ganse et al., 2012]. The PIC simulations are computationally very demanding so usually the size of the simulation box is very small

and/or the number of spatial dimensions is less than three. In addition, unrealistic proton-to-electron mass ratios must often be used.

Test-particle In test-particle simulations the particles are propagated in given background fields with no back-reaction. This approach makes it possible to analyse for instance the particle acceleration in such spatially extended systems as coronal shocks [Sandroos and Vainio, 2009]. Monte Carlo methods are often employed to account for the effects of fluctuating fields [e.g., Vainio et al., 2000].

Naturally the list above is not exhaustive and there are numerous combinations of the methods. For instance the test-particles can be propagated in background fields that have been calculated using a PIC simulation [Yang et al., 2009].

In **Paper II** we used a test-particle simulation to further investigate particle acceleration in the IP shock – bow shock interaction event described in **Paper I**. The energetic protons were injected in the energy range 0.1–3 MeV, with characteristics matching the observations, and propagated as guiding centres in the simulation box that was a quasi-two-dimensional slab with periodic Z-boundaries. The IP shock was treated as a planar discontinuity similarly to, e.g., Sandroos and Vainio [2006]. Its downstream plasma properties were calculated analytically using the Rankine-Hugoniot jump conditions (Equations (2.10)–(2.14)) in the infinite Mach number limit but keeping the compression ratio as a free parameter. To be compatible with the guiding centre approach, the fields near the IP shock were modified (widened) to increase linearly from the upstream to the downstream value, as opposed to a sharp step-function. This widening of the front was needed for the guiding centers within one gyroradius of the front to interact with it. The bow shock of the Earth was modelled as a paraboloid using the empirical model by Merka et al. [2005], with the magnetosheath cut out from the simulation region.

We did not include any scattering in our model, so the test-particles were accelerated only by the Shock Drift Acceleration. At the IP shock this was produced by the widening of the shock front decribed above and the non-inertial effects taken into account in the particle propagation scheme. We compared the particles' energy gains $\Delta U/U_0$ produced by the IP shock scheme (initial energies $U_0 \in [1, 10, 100, 1000]$ keV, $V_{\rm sh} = 350$ km/s and $r = 3.25$) with the analytical solution of Webb et al. [1983]. We obtained an excellent agreement with the analytical solution except for the lowest test energy, which was well below the energy range considered in the study proper.

For the acceleration at the bow shock we used a more complex model: the particles were either reflected or transmitted in the local dHT frame depending on their pitch-angle, without drifting on the bow shock surface. The bow shock compression ratio, which influences the reflection via the downstream magnetic field, was taken to depend on the position along the bow shock surface, decreasing towards the tail. Transmitted ions were removed from the simulation.

By using the pre-accelerated, energetic seed population arising from the observations of **Paper I**, we were able to avoid the so-called injection threshold problem [e.g., Lembege et al., 2004]. In order to reflect from the shock and escape upstream, a particle needs high enough initial energy, otherwise it is transmitted to the downstream. Namely, its velocity parallel to the magnetic field should exceed the speed of the shock–field line intersection: $V_{1\mathrm{n}}/\cos\theta_{Bn}$. The velocities of the thermal solar wind particles are much smaller than the threshold velocities of typical space plasma shocks, leading to both practical and fundamental problems for many shock acceleration studies.

Chapter 3

Shock Observations: Selected Topics

Shock observations and the supporting simulations have been reviewed many times during the satellite era. A comprehensive review has recently been written by Treumann [2009]. The results of the early phase of the Cluster mission have been discussed in the context of previous studies in Balogh et al. [2005], Bale et al. [2005], Burgess et al. [2005], and Eastwood et al. [2005] (see also Schwartz [2006]). Interesting insight into the observations on the Earth's quasi-parallel bow shock is given in Wilkinson [2003].

This chapter draws from these reviews along with additional studies to provide an introduction to the topics of this thesis. Section 3.1 gives an overview of the structure of the shock front at different scales. Section 3.2 presents in more detail the foreshock region upstream of the shock that affects the quasi-parallel shock structure to such a degree that they cannot be treated separately. Section 3.3 addresses the magnetosheath region between the bow shock and magnetosphere of the Earth. We concentrate on the status of the field related to the fast magnetosheath jets that were studied in **Paper III** and **Paper IV**. Last, in Section 3.4, we review the studies of particle acceleration in shock–shock interaction preceding those of **Paper I** and **Paper II**.

A problem related to spacecraft studies of space plasma shocks is that the vast majority of observations are of the bow shock of the Earth. At this shock so close to home, we can access a wide range of plasma conditions with a reasonable effort. However, the effects of its relatively small scale should be borne in mind when making conclusions about shocks in general, as illustrated in the following sections.

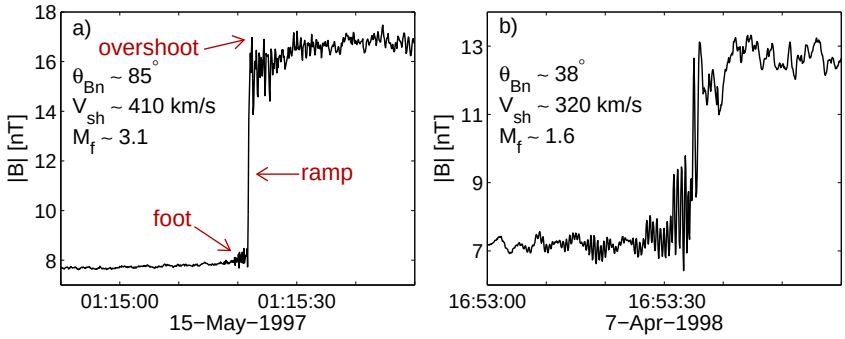

Figure 3.1: Wind 10.9-Hz resolution magnetic field measurements of (a) quasi-perpendicular and (b) quasi-parallel interplanetary shock crossings. The shock obliquity, speed, and fast-wave Mach number are indicated in the figure.

3.1 Shock structure and geometry

Figure 3.1 shows Wind 10.9-Hz resolution magnetic field measurements of two interplanetary shock crossings: a quasi-perpendicular shock on May 15, 1997, and a quasi-parallel shock on April 7, 1998. The depicted time interval is the same 1 minute for both crossings.

The crossing of the interplanetary shock with $\theta_{Bn} \sim 85°$ (Figure 3.1(a)) shows the main ion scale features of the shock structure: the foot, the ramp, and the (weak) overshoot. Before briefly presenting the quite well-known ion dynamics responsible for these features, we would like to note that the electron dynamics and smaller scale features still remain poorly understood. Schwartz et al. [2011] were only recently able to resolve the electron temperature gradient of the quasi-perpendicular bow shock using Cluster measurements: half of the electron heating coincided with a thin layer only several electron inertial lengths thick.

The shock *ramp* is the region of steepest spatial gradients. The steepening is limited and balanced by dispersion and/or dissipation. The nature of the dissipation differs according to the shock Mach number, and is still under active research as discussed in Section 2.2. This balance defines the width of the shock front and in particular the ramp. Bale et al. [2003] used Cluster spacecraft potential measurements—a common high time-resolution proxy for plasma density—to determine the ramp scale in 98 quasi-perpendicular bow shock crossings. They found that the natural scale of the transition is the convected ion gyroradius, i.e, the ratio between

the shock speed in the plasma frame and the downstream ion cyclotron frequency, especially at higher Mach numbers.

Space plasma shocks are often supercritical, i.e., they have a Mach number so large that in theory, the anomalous resistivity is unable to convert the required amount of energy from bulk flow into thermal energy [Kennel et al., 1985]. At supercritical quasi-perpendicular shocks, a part of the incoming ion population is reflected at the ramp due to a combination of magnetic forces and an electrostatic cross-shock potential. These reflected ions gyrate around the magnetic field in the immediate upstream of the shock front (see Figure 2.3), where they form the *foot* structure [e.g., Livesey et al., 1983]. When they re-encounter the shock they are either reflected again or have gained sufficient energy from the convective electric field to pass through the shock layer. In the downstream shocked plasma these ions then contribute to the *overshoot* and to a possible undershoot. For information on the absolute scales of these structures, see Bale et al. [2005].

Though shock waves are often considered stationary, observations and simulations have revealed that, on the contrary, a supercritical shock front is intrinsically non-stationarity (for a historical review, see Bale et al. [2005]). In particular, the quasi-periodic self-reformation of supercritical quasi-perpendicular shocks due to reflected particles has attracted considerable interest [Treumann, 2009]. However, this small scale rippling of the shock front is beyond the scope of this work.

The crossing of the interplanetary shock with $\theta_{Bn} \sim 38^\circ$ (Figure 3.1(b)) illustrates the spatially extended and more turbulent nature of a quasi-parallel shock transition. At quasi-perpendicular shocks the effects of the reflected ions were mostly restricted to the shock foot. Under quasi-parallel geometry ions that are either reflected or escaping from the downstream can travel upstream (Figure 2.3) and populate a much larger region. The region magnetically connected to the shock and filled with backstreaming particles is called the *foreshock*. Due to the counter-streaming particle populations the foreshock is subject to a number of instabilities that can grow into large amplitude magnetic fluctuations. Accordingly the variability of quasi-parallel shocks is rather the norm than the exception [Schwartz, 2006]. The bow shock observation-based current view of the quasi-parallel shock transition will be discussed more in the next section together with the associated zoo of foreshock phenomena.

Moving on to even larger scales, the curvature of the shock front plays a major role especially in planetary bow shocks. Figure 2.2(a) illustrates the main features of the bow shock of the Earth (labelled B in the figure). The magnetopause (A) separating the magnetospheric plasma from the shocked

solar wind plasma of the magnetosheath is usually located at a distance of $10\,R_{\mathrm{E}}$ in the solar direction. The bow shock is curved at magnetospheric scales while the structures in the solar wind and interplanetary magnetic field are typically large compared to the size of the magnetosphere. Hence the locations of parallel (C) and perpendicular (D) regions of the bow shock vary depending on the direction of the IMF. In turn, the position of the bow shock and the magnetopause vary in response to the solar wind dynamic pressure and Mach number.

The particles that reflect from the quasi-perpendicular side of the bow shock propagate upstream along the magnetic field lines. At the same time, the cross-field drift of the solar wind convective electric field acts to convect the escaping particles back towards the bow shock. How much the particle is deviated depends on its velocity. This results in a 'velocity-filter' effect: the trajectories of particles originating from one location on the bow shock are dispersed according to their velocity. Consequently, the electron (E) and ion (F) foreshocks of the bow shock are formed as illustrated in Figure 2.2(a) as a combined effect of particles originating from different regions along the bow shock.

The curvature together with the foreshock formation leads to different particle acceleration mechanisms being effective in different bow shock regions. Energetic particle observations made immediately upstream of the bow shock seem to be consistent with diffusive acceleration at the quasi-parallel region and shock drift acceleration at the quasi-perpendicular region [Meziane et al., 2002]. The maximum energies are limited by the small size of the bow shock, as the particles convect past it [e.g., Krauss-Varban, 2010]. These characteristics have bearing on the particle acceleration studies of **Paper I** and **Paper II** where the bow shock was one of the two interacting shocks.

Kennel et al. [1984a] pointed out that the bow shock's radius of curvature is smaller than the length scale of the foreshock. Moreover, the turbulence in the quasi-parallel magnetosheath extends to the magnetopause, and hence it is difficult to estimate its decay length. Consequently, they argued that the bow shock is not perfectly separated from the magnetopause. Combined with the motion of particles from the quasi-perpendicular side to the quasi-parallel side via foreshock, some features of the bow shock may be very different from other shocks with better scale separation.

For instance, though no significant turbulence or secondary ion acceleration is seen farther upstream of the quasi-perpendicular bow shock due to the convection, these are present at (oblique) interplanetary shocks [Desai et al. [2011], Krauss-Varban [2010], and the references therein]. Krauss-Varban et al. [2008] performed large (hundreds of proton inertial

lengths) and long-duration ($300\,\omega_{\rm cp}^{-1}$, $\omega_{\rm cp}$ is the proton cyclotron fryquency) 2D hybrid simulations of an oblique ($\theta_{Bn} = 50°$) planar shock. They found that the sufficiently large scale planar shock catches up with the dilute ion beams it has reflected, and is subject to the instabilities they create. In their simulation the compressional waves change the local θ_{Bn}—undulation with a wavelength of about 100 to 200 proton inertial lengths—resulting in more upstream wave and particle production.

Fortunately, with multi-point observations we are not as bound as the early missions by the assumptions of strict planarity of interplanetary shocks either. In fact, the assumption has been tested by Neugebauer and Giacalone [2005]. They analysed 25 well-defined quasi-perpendicular interplanetary shocks that had been observed by five spacecraft plus one event that had been observed by six. They used the four-spacecraft method to obtain five (fifteen in the six spacecraft event) independent sets of normals and speeds. They also calculated normals and speeds using single-spacecraft methods. Furthermore, they estimated the shock radius of curvature with different methods. Most of the shocks were inconsistent with planar structures, or spherical structures with a radius of 1 AU. In other words, the shocks were found to be rippled. They reported that the average local radius of curvature was $\sim 3 \times 10^6$ km ($\sim 500\,R_{\rm E}$) that is close to the observed coherence scale of the fluctuating IMF. Note that the size of the ripples they could observe was limited from below by the spacecraft separations, which were of the order of 10^5 km, corresponding to 10^3 ion inertial lengths for typical solar wind conditions. Thus they were not able to discern any smaller scale ($\lesssim 10^2$ ion inertial lengths) ripples existing at the same time, though such were evident in the 2D hybrid simulations presented in the same article.

To summarise, many space plasma shocks show structuring at various spatial scales. Often the conventional plane wave description is not sufficient, and should at least be carefully tested. The shock front rippling also casts some doubts to conclusions drawn from single spacecraft observations of, e.g., shock obliquity versus foreshock formation.

3.2 Wave-precursors and foreshocks

As the overall radius of curvature of ICME and CIR-associated shocks is much larger than the bow shock's, they should in principle reveal the differences between the quasi-perpendicular and quasi-parallel geometries. The early observations [Kennel et al., 1985] revealed that wave-precursors extended hundreds of $R_{\rm E}$ upstream of quasi-parallel IP shocks, but not of quasi-perpendicular IP shocks (based on the instantaneous obliquity mea-

surements). Supra-thermal ions, on the other hand, were observed upstream of IP shocks with a wide range of θ_{Bn} [Gosling et al., 1984]. However, judging the global solar wind conditions is difficult and single point measurements of the shock parameters do not necessarily reflect the large scale physics, as discussed above. The study of interplanetary shock foreshocks has only recently re-activated owing to the STEREO mission. For instance, Blanco-Cano et al. [2011] have reported that at 1 AU, the ICME-driven shocks have more extended foreshocks than the CIR-related shocks.

The foreshock region of the bow shock is always present and easier to probe, but formed as an interplay between the quasi-perpendicular and quasi-parallel regions, as noted in the previous section. Yet its role in the solar wind–magnetosphere interaction certainly warrants dedicated studies of its properties. The recent presentation of Cluster foreshock results by Eastwood et al. [2005] includes also an extensive list of previous reviews of foreshock studies. Here we will concentrate on the foreshock phenomena relevant to the studies of this thesis and the related recent findings.

The location of the foreshock varies according to the interplanetary magnetic field direction. Of special interest to foreshock related studies is the radial IMF configuration, i.e., the geometry when the magnetic field is (locally) parallel to the Sun–Earth line. More quantitatively, the IMF is typically considered quasi-radial if the angle between $\mathbf{B}$ and the Sun–Earth line (the cone-angle) or the angle between $\mathbf{B}$ and $\mathbf{V}_{\mathrm{SW}}$ is less than 30°. According to statistical studies, radial IMF is observed 16% of the time [Suvorova et al., 2010] and extended ($\geq 6\,\mathrm{h}$) periods occur at the wake of every fifth ICME [Neugebauer et al., 1997].

During radial IMF, the subsolar bow shock is quasi-parallel and thus the foreshock covers the whole dayside and extends far to the upstream solar wind. Accordingly many foreshock related phenomena are the strongest under these conditions [e.g., Blanco-Cano et al., 2009, and the references therein]. Consequently radial IMF is favoured in foreshock simulation studies. We will also return to the radial IMF in the next section when discussing the anomalous magnetosheath flows.

The reflection and energisation of particles at the bow shock depend on the shock obliquity and Mach number that vary rapidly along the shock front. Combined with the 'velocity-filter' effect, different parts of the foreshock are populated with different types of particles and accompanying waves leading to spatial regions with rather distinct characteristics [Eastwood et al., 2005]. The locations of electron and ion foreshocks for a tilted IMF direction are illustrated in Figure 2.2(a). Furthermore, a number of ion groups have been named based on their observed velocity distribution characteristics [e.g., Kis et al., 2007, and the references therein]. For

example, 'field-aligned ion beams' are observed near the leading edge of the ion foreshock, while 'intermediate' (a crescent-like shape) and 'diffuse' (a wide, fairly isotropic shell) ions are seen deeper in the ion foreshock, upstream of the quasi-parallel bow shock. The latter two populations are observed together with ultra low frequency (ULF) waves (0.01–0.2 Hz). Accordingly, this region of wave activity is confined by the ULF wave boundary. A newer finding is the foreshock compressional boundary associated with enhanced densities and magnetic field strengths [Sibeck et al., 2008; Omidi et al., 2009]. Its formation is tied to the ULF wave activity, but the compressional nature can be understood in terms of the backstreaming ions resulting in increased pressure within the foreshock and leading to expansion against the pristine solar wind. For low cone-angles, the compressional boundary is symmetric with the Sun–Earth line, while at larger cone-angles it forms only on one side.

Some of the foreshock waves can steepen into larger structures, such as Large Amplitude Magnetic Structures (SLAMS) [Schwartz and Burgess, 1991] (or simply 'pulsations' [Burgess, 1995]) that convect back to the bow shock and modify it. The SLAMS have a relatively smooth magnetic field signature, where the magnetic field magnitude is enhanced by a factor of two or more over the background level. For an early statistical study see, e.g., Mann et al. [1994]. Schwartz and Burgess [1991] suggested that SLAMS coalesce together to form the quasi-parallel shock front. Yet not all quasi-parallel shocks fit this 'patchwork scenario' [Burgess, 1995].

Based on the early single and twin spacecraft studies it was suggested that SLAMS would be of the order of 0.5–1 R_E in scale [Schwartz, 1991]. Cluster observations at $\sim$ 1000 km spacecraft separations indicate that SLAMS are coherent transverse to the expected shock normal over these scales [Lucek et al., 2008]. However, somewhat unexpectedly, smaller separations showed that even at scales of 600 km, SLAMS appear to be structured instead of monolithic [Lucek et al., 2002]. Only at scales of 100 km, comparable with the ion inertial length in the pristine upstream solar wind at the time, the SLAMS showed more coherence [Lucek et al., 2004]. Lucek et al. [2004, 2008] argued that the structuring is spatial rather than temporal, implying that SLAMS are quite filamentary in nature [Schwartz, 2006]. On the other hand, a filamentary structure agrees well with the recent simulations [Omidi et al., 2005, 2009; Blanco-Cano et al., 2006, 2009; Lin, 2003]. All in all, satellite observations and simulation studies have led to the picture of quasi-parallel shock being an extended region highly varying in space and time.

Foreshock influence is not limited to SLAMS. The ubiquitous variations in the solar wind properties, particularly in the IMF direction, lead to

transient phenomena in the foreshock. For instance, Turner et al. [2011a] have reported THEMIS observations of a magnetopause disturbance that was probably caused by a foreshock cavity that was formed at the edge of the foreshock as the IMF changed direction.

One of the most spectacular transient phenomena are the Hot Flow Anomalies (HFAs) (for a review, see Facskó et al. [2010]). In the 'classic' scenario, HFAs are formed when a tangential discontinuity under suitable solar wind conditions sweeps across the bow shock from the perpendicular to the parallel side. The change in the IMF direction should be such that the solar wind convective electric field is directed towards the discontinuity on at least one side of the TD. The field focuses the reflected particles and they can be channelled along the discontinuity plane. This leads to a disruption in the bow shock, and to the emergence of a bulge of hot magnetosheath-like plasma by the time the TD reaches the quasi-parallel region. The ion distributions inside the bulge are complex and the bulk flow velocity is often low or even sunward. The magnetopause as well can be locally pulled sunwards [Jacobsen et al., 2009]. Interestingly, Zhang et al. [2011] have recently reported THEMIS observations indicating that HFAs could also grow out of foreshock cavities.

Another newly discovered transient with global effects is the foreshock bubble [Omidi et al., 2010; Turner et al., 2011b], which is formed as a rotational discontinuity traps the backstreaming ions in the foreshock during small cone-angles. As the bubble smashes into the bow shock, it has global magnetospheric effects as the flow in the magnetosheath is momentarily reversed.

3.3 Anomalous magnetosheath flows

The sheath region between the shock and its driver, be it the magnetopause or a magnetic cloud, is as dynamic as the upstream region. Here again, the magnetosheath of the Earth is the most extensively studied sheath region [Lucek et al., 2005]. On average, the magnetosheath properties show spatial ordering imposed by the shape of the magnetopause as well as variations that depend on the solar wind input. Yet our understanding of how the bow shock processes the upstream variations, especially the foreshock phenomena generated by itself, is still quite poor. Recently, as the multipoint observations of Cluster and THEMIS on the dayside have accumulated, the complex magnetosheath structures have come under active research.

One of these intriguing phenomena are the anomalous magnetosheath flows with high dynamic pressure that we studied in **Paper III** and **Paper IV**. Although it is not possible to ascertain that all reported en-

hancements of *flux* [Nemecek et al., 1998], *kinetic energy density* [Amata et al., 2011; Savin et al., 2008, 2011, 2012], *velocity* [Shue et al., 2009] or *dynamic pressure* [Archer et al., 2012] would indeed be the same phenomena, they seem to share similar characteristics. The *jets*, as we have opted to call them, have a finite spatial scale of the order of a few R_{E}. Nemecek et al. [1998], who made the flux enhancement observations near the flank magnetopause, reported no significant variations in velocity, though the data points were sparse. The pressure pulses observed by Archer et al. [2012] were fast, but generally not supermagnetosonic, while the jets observed by Shue et al. [2009], Amata et al. [2011], and Savin et al. [2008, 2011, 2012] were. The dynamic pressure of the jets clearly exceeds the ambient dynamic pressure of the magnetosheath, and typically the dynamic pressure of the pristine solar wind as well. The jets seem to occur behind a quasi-parallel shock [Amata et al., 2011; Archer et al., 2012] and in particular, during radial IMF [Nemecek et al., 1998; Shue et al., 2009].

Before **Paper III**, no mechanism was proposed for the formation of the magnetosheath jets. Reconnection had been ruled out by Nemecek et al. [1998] and Savin et al. [2008] (also later in a careful study by Amata et al. [2011]). The MHD and hybrid simulations of Lin et al. [1996a,b] had shown that solar wind rotational discontinuities would form pressure fronts in the magnetosheath with amplitudes 2–3 times the background magnetosheath pressure. Nemecek et al. [1998] pointed out that these fronts were inconsistent with the observed finite spatial scale. They suggested locally created foreshock discontinuities instead, although the foreshock observations they presented did not correlate with the magnetosheath observations.

In **Paper III** we pointed out that local changes in the curvature of a high M_{A} shock front can result in fast bulk flows on the downstream side. Based on observations and simulations [e.g., Lucek et al., 2008; Omidi et al., 2005; Blanco-Cano et al., 2009], it seems that such ripples are inherent to quasi-parallel shocks. In brief, we noted that in the regions where the local shock normal is quasi-perpendicular to the upstream velocity, the shock mainly deflects plasma flow while the speed stays close to the upstream value. Together with the compression of the plasma, these localised streams can lead to jets with a dynamic pressure that is several times higher than the dynamic pressure in the upstream region. Naturally, it is not possible to verify that all reported jets would stem from the shock-ripple-related mechanism.

Later, Savin et al. [2011, 2012] have claimed that many jets would be flow deflections due to Hot Flow Anomalies. However, no significant velocity enhancements are seen in the typical HFA crossings [Facskó et al., 2010, and the references therein]. Compression regions, on the other hand,

are formed on the edges as the HFA expands in the direction transverse to the flow.

Recently, Archer et al. [2012] returned to the propositions of Lin et al. [1996a,b] as they studied THEMIS observations of dynamic pressure pulses. Many of the pulses were adjacent to large rotations in the magnetic field direction, though not all of them could be unambiguously associated with solar wind discontinuities. They proposed that the pulses would be triggered by a very specific subset of discontinuities changing the bow shock local obliquity from quasi-perpendicular to quasi-parallel, or vice versa. During such transitions, no pulses were observed downstream of the quasi-perpendicular bow shock. Consequently, they suggested that the quasi-parallel region could play a role in the pulse formation. In particular, the breaking up of the pressure front seen in the simulations [Lin et al., 1996a,b] into the observed smaller pulses could be related to the SLAMS. We will discuss these propositions more in the context of **Paper III** and **Paper IV** in the next chapter.

In **Paper IV** we also studied how these 'local' mesoscale variations affect the magnetosphere. The jets with their high dynamic pressure provide a source for large magnetopause perturbations [Shue et al., 2009; Amata et al., 2011; Archer et al., 2012]. The favourable conditions for the occurrence of jets—radial IMF and/or downstream of a quasi-parallel bow shock—are in fact the same as for the occurrence of magnetopause perturbations [Russell et al., 1997; Plaschke et al., 2009]. Furthermore, these conditions also agree with observations of magnetic oscillations at the geostationary orbit during steady solar wind [Sanny et al., 2002].

On the other hand, the density variations in the foreshock of a quasi-parallel bow shock that can contribute to the shock rippling have been suggested to transmit into the magnetosheath and impinge on the magnetopause [Sibeck et al., 1989; Fairfield et al., 1990]. However, the foreshock dynamic pressure variations are typically much smaller than the pulses in the magnetosheath [Sibeck et al., 1989; Archer et al., 2012]. The bow shock ripples could thus act as amplifiers of the upstream variations, and the ripple induced jets could then be a means to transmit the variations through the magnetosheath and effectively perturb the magnetopause.

3.4 Particle acceleration in shock–shock interaction

While most studies consider particle acceleration in a single shock (see, e.g., the reviews by Burgess [2007] and Reames [1999] for the bow shock and

the inner heliosphere), shock–shock interaction is an interesting topic as well. In **Paper I** and **Paper II** of this thesis, we addressed the question of acceleration in a head-on collision of two shocks. This acceleration setup has its roots in the work by Fermi [1949], as discussed in Section 2.2.2; a geometry where two shocks collide head-on establishing a contracting magnetic bottle, is an evident way to produce enhanced acceleration.

In the solar system, suitable configurations can form when a CME-driven shock hits a planetary bow shock or a CIR shock. In fact, Gómez-Herrero et al. [2011] have reported observations of possible interplanetary CME–CIR interactions affecting the observed energetic ion fluxes at 1 AU. It has also been suggested [Giacalone et al., 1993; Mann et al., 1994; Classen and Mann, 1998] that SLAMS in the foreshock of the Earth's bow shock could act as small, shock-like magnetic mirrors and accelerate particles as they convect to the bow shock.

Previous observations of particle acceleration in shock–shock collisions have been mostly indirect. The interaction of two CMEs, for instance, has usually been inferred by combining white-light coronagraph images taken by LASCO (onboard SOHO spacecraft) with radio observations. For a recent summary see, e.g., Lugaz et al. [2008]. Before **Paper I**, *in situ* observations had been reported on two events of IP shock interaction with the bow shock of the Earth: one on November 11–12, 1978, and the other on October 18, 1995.

The interplanetary shock event of November 11–12, 1978, has been entitled as "the grandaddy of all quasi-parallel interplanetaries", as it was i) one of the strongest solar energetic particle events observed at the time and ii) the first IP shock for which a wave-precursor was found [Kennel et al., 1984b]. Scholer and Ipavich [1983] compared the flux of 30–157 keV ions observed by ISEE-1 during the event close to the quasi-perpendicular bow shock to the flux observed by ISEE-3 far upstream. In particular, ISEE-1 detected a peak-like enhancement of the flux at the IP shock crossing, but this peak was not seen in the ISEE-3 profiles. They interpreted the peak to result from particles upstream of the IP shock undergoing further acceleration at the bow shock. In addition, Kennel et al. [1984b] suggested that the pressure of the suprathermal protons was as high as the thermal and magnetic pressure upstream of the IP shock at ISEE-3, even though the spacecraft was not connected to the bow shock.

Reacceleration of energetic electrons in the event of October 18, 1995, was briefly reported by Terasawa et al. [1997]. The setup was very similar to the event of November 11–12, 1978: Geotail was approximately $10\,R_{\mathrm{E}}$ upstream of the nominal (quasi-parallel) bow shock location while Wind was located far upstream ($X_{\mathrm{GSE}} \sim 175\,R_{\mathrm{E}}$). Geotail observations showed

evidence of bi-directional electron anisotropy along the IMF. According to the interpretation of Terasawa et al. [1997], the bow shock and the IP shock were magnetically connected for 50 min before the crossing, and the electrons trapped between them were accelerated.

Including the event of August 9–10, 1998, studied in **Paper I** increases the number of analysed IP shock–bow shock interaction events to three. It would thus seem that, despite being quite a common phenomenon in space, shock interaction events with both magnetic field *and* spacecraft configurations suitable for detailed *in situ* studies are relatively rare. Besides, as the shocks are curved, the angle θ_{Bn} at both connection points of the spacecraft should be carefully inspected.

Shock–shock collisions have been investigated in a few simulation studies as well. Cargill [1991] (see also the first article in the series Cargill et al. [1986]) used a 1D hybrid code to test the effects of the shock obliquity (θ_{Bn}) and the relative strength of the two shocks on particle acceleration. It should be noted that these simulations dealt with very small spatial and temporal scales: for typical solar wind conditions at 1 AU the simulation parameters correspond to a box size of about 1–3 R_{E} and a duration of 10–30 s. In order to overcome the difficulty related to the formation time of a steady-state shock front, both shocks were initialised separately and then loaded into the common simulation box. The particles were accelerated out of the thermal population. Their energies reached 10 and 30 times that of the kinetic energy of the unshocked ions for quasi-perpendicular and quasi-parallel shock pairs.

Recently, Lembège et al. [2010] have analysed collisions between quasi-perpendicular non-stationary shocks using a 1D full particle-in-cell simulation. Their main interest, however, was not particle acceleration but shock front self-reformation before and after collision.

Interestingly, particle acceleration in shock–shock collisions, or rather, in shock merging has been studied also in the laboratory. A series of papers including Dudkin et al. [1992, 1995, 2000] concerning collisionless proton and deuteron plasmas was produced with the motivation to investigate the possibilities of shock-based particle accelerators. They used a specific geometry where two quasi-perpendicular, low Alfvén Mach number shocks collided at a fixed angle, so that the background magnetic field lay between the shock fronts. The energy of the accelerated deuterons streaming along the magnetic field reached 1–10 MeV.

Chapter 4

Results

This chapter describes the main results of the four articles together with some further analysis as well as discussion in the context of recent developments in the field. Section 4.1 presents the multi-spacecraft study of particle acceleration in shock–shock interaction followed by further analysis with a numerical model. The novel result was the first *in situ* observations of particles released as the shocks collide—an interpretation that was further confirmed by the simulation study. Section 4.2 describes the studies on high speed subsolar magnetosheath jets: a mechanism for their formation, their observational properties, as well as effects on the magnetosphere. We found that the proposed mechanism based on the bow shock ripples can account for the main properties of the jets, including their finite spatial scale and the observed range of dynamic pressure. The signatures of the jets could also be identified at the geostationary orbit and in the ionosphere.

4.1 Shock–shock interaction

Particle acceleration in shock–shock interaction is a well-established acceleration mechanism, but difficult to identify from observations. Figure 4.1(a) illustrates an ideal setup: two quasi-parallel shocks approach each other forming a contracting magnetic trap. Particles with a small enough pitch-angle are able to escape the trap. The rest of them gain energy through interaction with the shocks and the conservation of the second adiabatic invariant. The acceleration mainly increases the momentum of the particles parallel to the magnetic field. Thus their pitch-angle decreases and at some point they, too, will be able to escape the trap.

Eventually the separation between the shocks becomes of the order of the gyroradius of the particles. The remaining particles will no longer feel

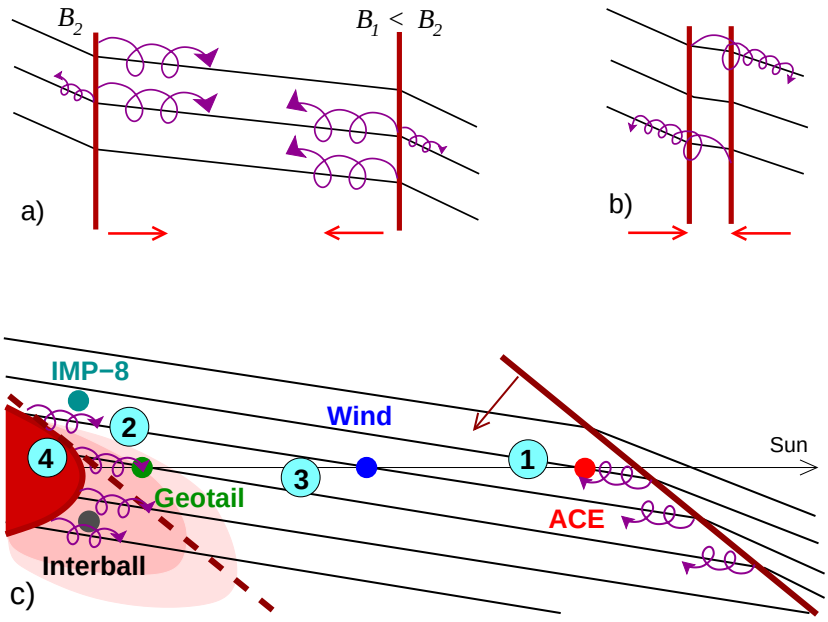

Figure 4.1: (a) Illustration of a magnetic trap formed by two shocks. The black lines depict the magnetic field, red lines the shock fronts and magenta spiralling arrows propagating energetic particles. (b) When the shocks get close enough to each other, the remaining particles escape. (c) Schematic picture of the August 9–10, 1998 event. The black lines depict the IMF. The red paraboloid represents the bow shock of the Earth, and the pink region its foreshock. The red line represents the IP shock, and the red dashed line indicates its the position when it hit the bow shock. The numbers refer to the different phases of particle acceleration (see text for details). Subfigure (c) adapted from **Paper II**.

the trap and are released, as illustrated by Figure 4.1(b). Since the gyroradius depends on the energy of the particles, the higher energy particles are released earlier than the lower energy particles.

Figure 4.1(c) presents the general geometry of the IP shock–bow shock interaction event of August 9–10, 1998, studied in **Paper I** and **Paper II**. The detailed analysis was made possible by the advantageous spacecraft configuration, and the quasi-radial IMF that lasted for several hours before the IP shock passage during the first hour of August 10.

4.1.1 Observations

The five spacecraft—ACE, Wind, IMP-8, Geotail, Interball—observations of the IP shock of August 10, 1998, was first used by Szabo [2005] to compare the normals obtained with the four-spacecraft method (Section 2.3.2). He concluded that the IP shock had ripples of the order of 1 R_{E}, but he did not take into account that the fifth spacecraft, Interball, was located deep in the foreshock region.

Prech et al. [2009] presented a "preliminary analysis" on the IP shock propagation through the foreshock in this event. They compared the magnetic field and plasma observations of the five spacecraft as well as the energetic particle measurements of Geotail and Interball near the IP shock crossing. They showed that "the profiles of basic parameters can be substantially modified, probably due to presence of energetic particles" in the foreshock. However, they did not discuss the possibility of enhanced acceleration due to shock–shock interaction. Thus they did not connect the high level of the energetic particles observed in the foreshock region to that process. In addition, they did not comment on the peculiar behaviour of the Geotail's omni-directional energetic particle measurements: the lower energy particles peaked at the IP shock crossing, the higher energy particles after the crossing.

In **Paper I** we compared the magnetic field, plasma, and energetic ion data from ACE, Wind, and Geotail spacecraft from August 9 00:00 UT to August 10 06:00 UT. We found that 17:00–19:00 UT on August 9, a tangential discontinuity crossed the near-Earth space. The IMF turned quasi-radial and kept this direction until the IP shock crossing on the next day. At the TD there was also a significant increase in the energetic particle fluxes. We found that the period of quasi-radial IMF corresponded to a flux tube that was connected to the IP shock and filled with a seed population of energetic particles accelerated by it (phase 1 in Figure 4.1).

Since ACE was magnetically connected to the IP shock but not to the bow shock, the seed population could be characterised by its measurements:

a constant spectral index and temporally constant flux intensity profiles during the 6–7 hours from the TD crossing to the IP shock crossing. No 'shock-spike' could be identified at the IP crossing. Thus ACE observations made it possible to distinguish the contribution of the bow shock and the shock–shock interaction to the particle acceleration. The energy channels above ~ 550 keV were particularly useful, as those energies are not normally seen upstream of the quasi-parallel bow shock even when there is an ambient seed population [Meziane et al., 2002].

Wind observed several particle bursts coming from the bow shock direction during the first part of the event (phase 2). These bursts corresponded to times when the spacecraft was connected to the quasi-perpendicular flank of the bow shock. Later, Wind became continuously connected to both shocks, and measured an increasing flux as well as two counter-streaming populations until the IP shock crossing (phase 3).

Geotail was located closest to the Earth and continuously connected to both the IP shock and the oblique bow shock. It recorded the highest intensity at the IP shock crossing. Adding directional information revealed that the peculiar peak had a complex structure: the fluxes of particles propagating parallel to the magnetic field (pointing out from the Sun) peaked before the IP shock crossing, with the higher energies leading. The fluxes of particles propagating anti-parallel to the IMF peaked approximately 2 minutes after the IP shock crossing and were responsible for the after-shock maximum of the omni-directional flux at energies larger than 140 keV. Moreover, also this peak of the sunward propagating particles seemed to occur for higher energies first, suggesting a source or a release anti-sunwards from the spacecraft. Based on this velocity dispersion and the analysis of the geometry of the two shocks, we concluded that these particles had been released from the magnetic trap between the shocks as they collided (phase 4).

Note that the magnetic connection of Geotail in this event differs from the connection of ISEE-1 in November 11–12, 1978, event. In particular, ISEE-1 was not connected to the bow shock during the half hour following the IP shock crossing [Scholer and Ipavich, 1983]. Consequently, it could not observe particles accelerated at the shock–shock intersection region. To our knowledge, we reported in **Paper I** the first direct, *in situ* measurements of particles released from the collapsing trap formed by two shocks.

The enhanced particle acceleration had interesting consequences for the foreshock. Figure 4.2 shows Interball measurements during the ~ 6 hours from the TD to the IP shock crossing. We can see that as the flux of ≥ 50 keV particles increased, the magnetic field magnitude and the anti-sunward flux steadily decreased well below the average solar wind level (blue

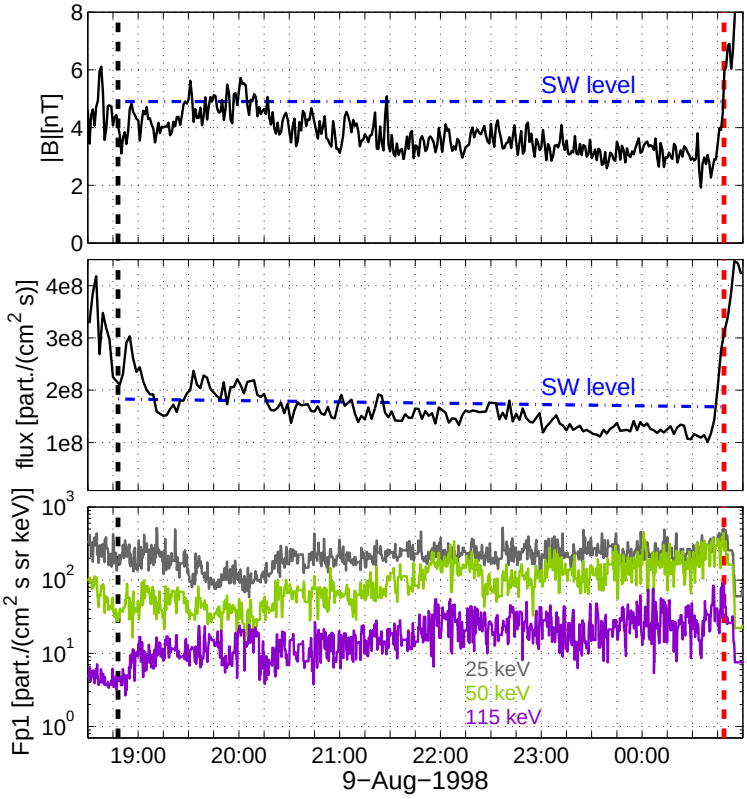

Figure 4.2: Interball observation in the foreshock during the shock–shock interaction event. From top to bottom: magnitude of the magnetic field, anti-sunward flux, and the energetic proton flux in three energy channels. The first proton sensor of the DOK-2 instrument looks anti-sunward. The vertical black and red dashed lines show the TD and IP shock crossings. The horisontal blue dash-dotted lines in the first two panels indicate the pristine solar wind level.

dash-dotted lines). Right before the IP shock the magnetic field magnitude was only 3 nT compared to the 5 nT of the pristine solar wind. Consequently the magnetic pressure in the foreshock was only one third of the magnetic pressure in the solar wind, but it was balanced by the increased pressure of the energetic particles. We conclude that the enhanced particle acceleration resulted in a diamagnetic cavity in the foreshock region of the Earth.

4.1.2 Simulations

In **Paper II** we used a global, 2.5D test-particle simulation described in Section 2.4 to further investigate particle acceleration in the August 9–10, 1998 event. In particular, we wanted to study the last hour of interaction when phases 3 and 4 were observed, to see whether the shock–shock interaction in this magnetic geometry could explain the observed shapes of the flux profiles.

We used ACE observations of the event seed population to characterize the test-particles. They were inserted into the box in the energy range 0.1–3 MeV and had a power-law energy distribution with the index $\sigma = -4$ and a step-function pitch-angle distribution. Furthermore, as the test-particle densities in the model are arbitrary, they were normalised so that the density in the 0.22–0.47 MeV range matched ACE observations in the beginning of the run.

Figure 4.3 shows two snapshots of the test-particle density in the energy range 0.22–0.47 MeV during the simulation run. The locations of Wind and Geotail projected to the equatorial plane are indicated as well. Figure 4.3(a) illustrates the processes taking place at the beginning of the run. The magnetic field lines connected to the dusk flank of the bow shock were filled with accelerated particles. As there was no scattering in the model, the quasi-parallel part of the bow shock did not accelerate particles and the pre-noon sector contained less particles than expected for the real foreshock region. The first particles reflected from the IP shock have formed a front (located near Wind in the figure) that proceeded through the box as the particles bounced between the shocks while drifting to the $-Y$ direction.

Figure 4.3(b) shows one of the main results of **Paper II**: at around 44 min the shocks begin to pass through each other starting from the post-noon region in this 2D projection. This results in a drop in the test-particle density. On one hand, this drop expands along the bow shock at the speed of the shock–shock intersections. On the other hand, the drop propagates downstream along the magnetic field lines at the speed of the last escaping

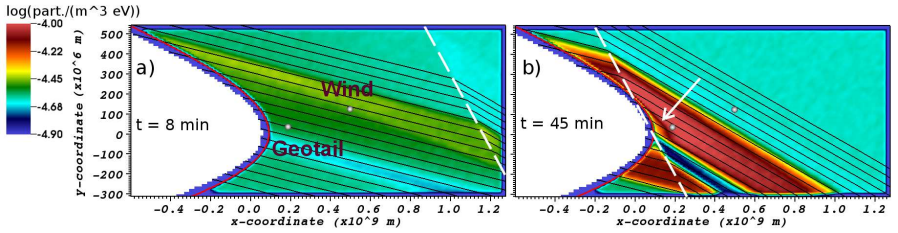

Figure 4.3: Snapshots of the test-particle density in the 0.22–0.47 MeV channel. The black lines indicate magnetic field lines. The red curve illustrates the location of the bow shock and the white dashed line the location of the IP shock. The white dots indicate the virtual spacecraft corresponding to Wind and Geotail. The white arrow points to the area of decreased particle density about to expand to the location of Geotail. Adapted from **Paper II**.

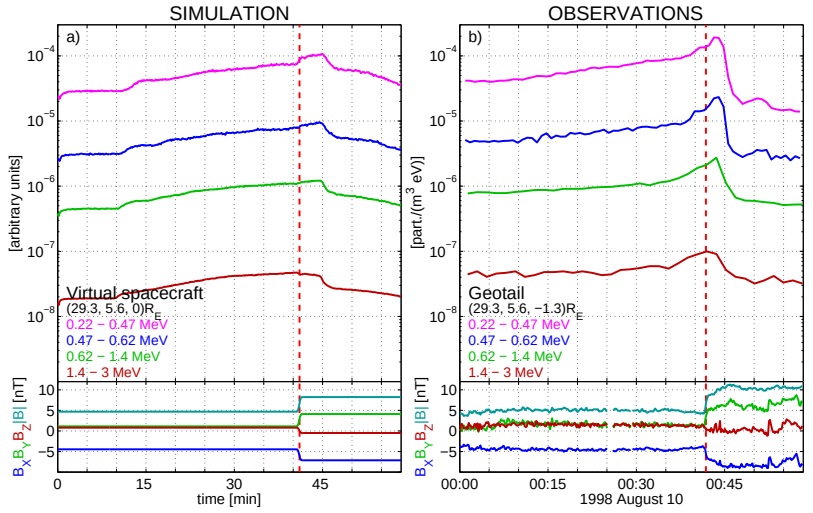

Figure 4.4: Comparison of energetic particle density time-profiles. The results of the numerical model are shown on the left (a), and the spacecraft observations on the right (b). In both cases the top panel shows the energetic particle density at four energy channels while the lower panel depicts the components of the magnetic field and its magnitude. The vertical red dashed line indicates the time of the IP shock crossing. The x-axis of (a) indicates the time since the beginning of the run, and the simulation clock has not been synchronised with the observations. Adapted from **Paper II**.

particles. The arrival of this drop to Geotail's location ends the increase in the test-particle density.

Figure 4.4 shows the simulated time series extracted from a virtual spacecraft placed at Geotail's location next to Geotail's actual observations. Note that in the model, the magnitude of the magnetic field after the IP shock crossing was $\sim 2\,\mathrm{nT}$ lower than observed due to small changes in the IMF direction just before the crossing. Before the crossing the simulated particle densities show a similar increase as the observations. Moreover, the maximum is reached after the crossing in both cases. The timing of the peaks, though not the height, is also very similar. As discussed above, this peak, or rather, the drop ending the increase was caused by the arrival of the decrease related to the shock collision. Since the last high energy particles reached the virtual spacecraft before the last low energy particles, the peak has a velocity dispersion of 30–50 s.

Despite the limitations of the model on the one hand and, e.g., the limited field-of-view of the spacecraft instruments on the other, we found a good agreement with the numerical model and the observations. To conclude, the simulation results verify that the main features of the measurements can be explained by shock–shock interaction in the magnetic geometry under consideration. In particular, they are in agreement with the interpretation given in **Paper I** that the Geotail post-shock maximum resulted from the release of particles from the collapsing trap.

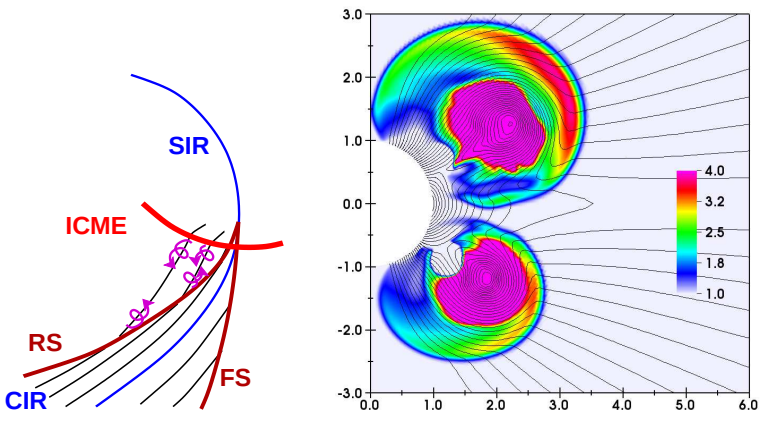

Figure 4.5: Left: Illustration of an ICME catching up a CIR. Right: Snapshot of an MHD simulation showing two consecutive CMEs lifting off at different angles. The colour-coding displays the compression ratio. Courtesy of J. Pomoell.

Shock–shock interactions in this type of magnetic geometries can occur in various space plasma and astrophysical settings, such as IP shock collisions with other planetary bow shocks. Another interesting case are ICME–CIR interactions, as illustrated on the left in Figure 4.5. An ICME catching up on a CIR can form a contracting magnetic bottle with the reverse shock. Gómez-Herrero et al. [2011] have reported on several STEREO observations of ICME–CIR interactions. In some of these events, the observed maxima in hundred-keV range particle fluxes could be related neither to shocks nor to developing shocks in the vicinity of the spacecraft. In **Paper I** we suggested that these enhancements could be caused by particles escaping from a trap between the ICME shock and the reverse shock beyond 1 AU. The right-hand part of Figure 4.5 shows a different setup where two CMEs lifting off at different angles form a trap between them. The upcoming Solar Probe Plus mission [07], approaching the Sun as close as 10 solar radii, may be able to provide more direct evidence of such interactions than the currect remote observations.

4.2 Supermagnetosonic magnetosheath jets

In **Paper III** and **Paper IV** we studied the near-Earth observations from the evening of March 17, 2007, which was characterised by an 8-hour period of steady solar wind with radial IMF. At 20:20 UT, the heliospheric current sheet crossed the Earth and the overall IMF configuration changed to more Parker spiral like. ACE and Wind were located near the L1 point and were used as solar wind monitors. Geotail was skimming the bow shock in the turbulent foreshock. The four Cluster spacecraft (C1–C4) were on an outbound orbit near the subsolar point. The magnetopause moved across them several times starting from 17:15 UT. The spacecraft constellation was flat in the nominal plane of the magnetopause, as C3 and C4 were close to each other (950 km apart), while the others were slightly more than 7000 km away.

The CIS-HIA instruments on C1 and C3 measured several antisunward jets with speeds between 300 and 500 km/s when the solar wind speed was 530 km/s. Although the duration of the jets varied, it should be noted that many of them lasted minutes. In other words, their spatial scale in the direction of the flow was several R_{E}, while the transverse size was (at least) of the order of the spacecraft separation. Thus the jets should be considered as a 'mesoscale' phenomenon, i.e., of a scale that is smaller than the global scale but larger than the kinetic scales.

In **Paper III** we proposed, based on the Cluster observations, a general plasma physics mechanism for the formation of fast, even supermag-

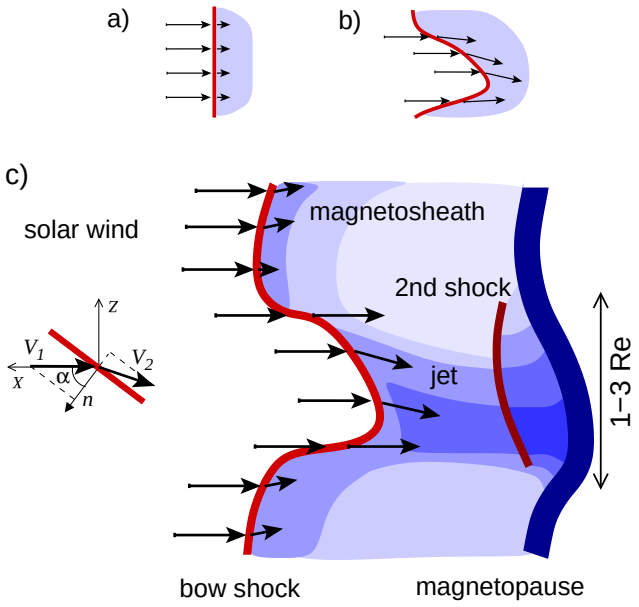

Figure 4.6: Top: Schematic picture of the velocity field across a high Mach number shock that is either planar (a) or rippled (b). The red line depicts the shock, and the blue area is the downstream side. Bottom: Illustration of the effect of a bow shock ripple. The variation of the plasma number density in the downstream region is illustrated by the shading: dark blue indicates density enhancement, light blue indicates density depletion. The jet perturbs the magnetopause depicted by the thick blue line. In the particular case where the jet is supermagnetosonic in the frame of the magnetopause, an additional weak shock forms. The inset details the flow deflection when $\mathbf{V}_1$ is not parallel to $\mathbf{n}$. Note that the picture is not to scale in the horizontal direction. Figure from **Paper IV**.

netosonic jets behind a rippled high Mach number shock. With a ripple we mean a local perturbation in the curvature of the shock front that changes the angle α at which the incoming flow meets the shock, as illustrated in Figure 4.6. We inferred that the lower limit for the scale of the particular jet and the bow shock ripple under consideration in **Paper III** was of the order of the spacecraft separation: $\gtrsim 50$ ion inertial lengths, $\sim$8000 km, $\sim 1.2\, R_{\rm E}$. Note that at kinetic scales the ripple most likely looks much more complex than Figure 4.6 indicates. Moreover, the ripples are highly dynamic.

In **Paper IV** we considered the properties of these magnetosheath jets and also extended the study to investigate their effects on the magnetosphere. For the latter purpose we used GOES-11 and 12 spacecraft that were in the geostationary orbit on the dayside. In addition, we analysed ionospheric velocity data measured by the SuperDARN radars in the Northern Hemisphere.

4.2.1 Mechanism

Let us first consider the plasma flow across a high $M_{\rm A}$ MHD shock wave. The shock primarily decelerates the component of the upstream velocity $\mathbf{V}_1$ that is normal to the shock front, i.e., the Rankine-Hugoniot jump conditions (2.10–2.14) give $V_{1\rm n} = rV_{2\rm n}$ and $V_{1\rm t} \approx V_{2\rm t}$. If the shock is planar, with an orientation illustrated in Figure 4.6(a), the density increase and the flow velocity decrease are $\rho_{m2} = r\rho_{m1}$, and $rV_2 = V_1$. The dynamic pressure of the plasma flow is thus smaller on the downstream side of the shock than on the upstream side:

$$P_{\rm dyn2} = \rho_{m2} V_2^2 = \frac{1}{r}\rho_{m1} V_1^2 = \frac{1}{r} P_{\rm dyn1}. \tag{4.1}$$

However, if the shock is locally rippled with a geometry sketched in Figure 4.6(b), the plasma speed stays close to the upstream value $V_2 \approx V_1$ near the edges of the ripple. Since the plasma is still compressed, $\rho_{m2} \approx r\rho_{m1}$, the dynamic pressure can in fact be larger on the downstream side than on the upstream side:

$$P_{\rm dyn2} \approx r\rho_{m1} V_1^2 = r P_{\rm dyn1}. \tag{4.2}$$

Figure 4.6(c) depicts a bow shock ripple that has a downstream flow profile matching the example jet considered in **Paper III** and **Paper IV**. Crossing the bow shock leads to efficient compression and deceleration of the solar wind plasma in the regions where the angle α between $\mathbf{V}_1$ and $\mathbf{n}$ is small. This is the typical situation near the bow shock apex. Still, if the

bow shock is locally rippled, there can be small regions where α is large, and the bow shock mostly deflects the solar wind flow.

The spatial profiles of the plasma parameters depend on the form (and the time development) of the ripple. The velocity maxima are found at the edges of the ripple, but the speed can be large at the centre as well. The density variations are caused by convergence and divergence of the flow, so that the maximum is near the centre of the ripple. There can also be additional plasma pile-up when the jet hits the magnetopause and indents it. This structuring of the magnetosheath is illustrated by the blue shading in Figure 4.6(c).

The high speed together with the increased density behind the ripple lead to a jet of very high dynamic pressure, as stated by Equation (4.2). The dynamic pressure of the jet perturbs the shape of the magnetopause. Furthermore, there is the possibility that the speed V_2 of this jet in the magnetosheath is still supermagnetosonic in the reference frame of the magnetopause. In this case a second weak shock front forms closer to the magnetopause (Figure 4.6(c)). In **Paper III** we identified such a secondary shock from the Cluster observations.

Radial IMF is not a favourable condition for the formation of (classic) Hot Flow Anomalies [Facskó et al., 2010], so the proposition of Savin et al. [2011, 2012] introduced in section 3.3 is not applicable to such events. For steady radial IMF Savin et al. [2012] suggest that foreshock disturbances would represent local obstacles for the solar wind flow and trigger jets similarly to the HFA case. However, as a part of their explanation they also invoke local conservation of the plasma flux (or flow), which is a quite problematic concept for collisionless plasmas, transient phenomena, and point measurements.

Archer et al. [2012] proposed, based on THEMIS observations and previous simulations [Lin et al., 1996a,b] that the dynamic pressure pulses would be caused by solar wind rotational discontinuities changing the bow shock from quasi-perpendicular to quasi-parallel, or vice versa. However, in **Paper III** and **Paper IV** we did not observe large enough or numerous enough variations in the IMF orientation to account for all the jets. Moreover, this proposition fails to explain the finite spatial scale of the pulses, as well as the observed range of dynamic pressure, as discussed in the next section.

4.2.2 Observational properties

In **Paper IV** we considered the general properties of the jets observed by Cluster on the evening of March 17, 2007. The Cluster configuration

discussed above was suited for studying the spatial scale of the jets transverse to the flow direction. Many jets were observed simultaneously by at least two Cluster spacecraft, so their minimum size was of the order of the spacecraft separation. The GOES-11 and 12 observations from the geostationary orbit showed corresponding magnetic field enhancements mainly for the spacecraft that was directly Earthwards of Cluster. We thus inferred that the jets were typically smaller than the GOES separation of $6\,R_{\mathrm{E}}$ transverse to the X_{GSE} axis. Most certainly the jets did not have a global spatial scale like, e.g., the foreshock bubbles do.

The main contribution to the jet speed came from V_X. The deflection, i.e., the sign of V_Y and V_Z, varied from one jet to another. These velocity characteristics support the mechanism proposed in **Paper III**.

Most of the jets had a dynamic pressure between two and four times the solar wind value, in agreement with Equation (4.2) and much larger than the pulses caused by RDs in the simulations of Lin et al. [1996a,b]. In a few cases, the pressure was as high as 5–7 $P_{\mathrm{dyn}}^{\mathrm{SW}}$. These extreme pulses coincided with density increases, possibly caused by convergence of the flow coming from different parts of the ripple or plasma piling up into a magnetopause indentation.

Archer et al. [2012] reported the magnetosheath dynamic pressure pulses to occur at 3–5 min intervals. Sibeck et al. [1989] studied 8-min variations, although it should be noted that they studied the possible transmission of foreshock pressure enhancements into the magnetosphere and not the pressure pulses in the sheath. In the event studied in **Paper III** and **Paper IV**, the jets do not appear strictly periodic. Rather, they seem to occur in bursts of larger and smaller jets. However, this may be the effect of one jet being sampled by a spacecraft several times when the jet moves in the magnetosheath.

One of the main features that sets the March 17, 2007, event aside from the jets and pressure pulses reported by the other authors [Shue et al., 2009; Amata et al., 2011; Savin et al., 2008, 2011; Archer et al., 2012] is the strength of the jets. Many of the jets had a $M_{\mathrm{MS}} > 1.5$ while those reported by others were only mildly supermagnetosonic or simply fast. The key difference could be the solar wind speed that was higher on March 17 than in the other events.

4.2.3 Magnetospheric effects

One of the goals of **Paper IV** was to study how the effects of jets were transmitted into the magnetosphere. Starting with the magnetopause, the high dynamic pressure of the jets provided an effective way to perturb its

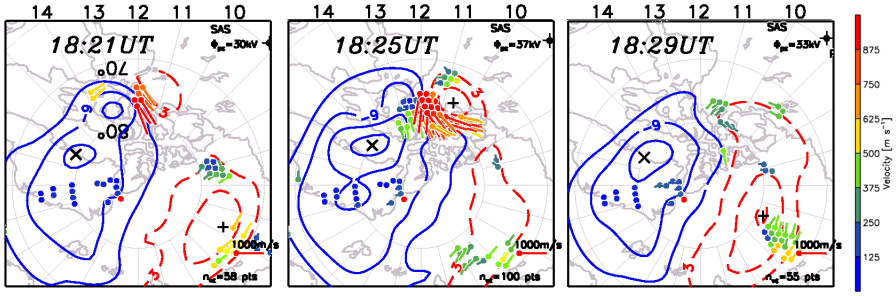

Figure 4.7: Ionospheric convection pattern fitted into the SuperDARN measurements. The maps are in magnetic coordinates and the Sun is to the top, dawn to the right, and dusk to the left in each panel. The maps represent the flow pattern with 2-min integration time at 18:20–18:22, 18:24–18:26, and 18:28–18:30 UT. Adapted from **Paper IV**.

shape. The magnetopause moved back and forth across the Cluster spacecraft as the jets pushed it Earthwards. Since the Cluster configuration was flat in the nominal magnetopause plane, it was not possible to measure the depth of the indentations. Shue et al. [2009] reported using the THEMIS pearls-on-a-string configuration that the depth of an indentation caused by a mildly supermagnetosonic jet was of the order of $1\,R_{\mathrm{E}}$. Thus the indentations in the March 17, 2007, event were probably deeper.

Even though we and the other authors have found magnetopause reconnection very unlikely as the cause of the high speed jets, local small-scale magnetopause reconnection as their consequence would not be surprising. It is quite plausible that the high dynamic pressure jets directed at the magnetopause and causing severe perturbations may also trigger small reconnection events.

Inside the magnetosphere, we considered data from the GOES-11 and 12 satellites in the geostationary orbit. They measured irregular pulsations when they were on the dayside during the period of radial IMF. We used the time interval that corresponded with the Cluster magnetosheath observations to determine the spatial scale of the jets as discussed in the previous section.

To investigate the ionospheric response to the magnetosheath jets, we examined the SuperDARN radar measurements of the ionospheric flow velocities. We identified localised and short-lived (on average $\sim$5 min) enhanced convection flow channels in the dayside polar ionosphere. Their

location and timing—each about 5 min after an intense jet—suggested that they were caused by the magnetosheath jets.

Figure 4.7 shows an example of such flow enhancement. The high speed flow started to appear at 18:20 UT in the region just Northwest of Hudson Bay. The flow channel was at its widest at 18:24 UT and there was an indication of a counterclockwise flow vortex. At 18:28 UT the flow signature had disappeared. We also examined the magnetometers of the CARISMA and CANMOS chains located under the field-of-view of the particular SuperDARN radar recording the main enhancement of Figure 4.7. The magnetometer data showed perturbations with a strength of 50–100 nT typical to mesoscale dayside variations [e.g., Kataoka et al., 2001, 2003] agreeing with the radar observations.

Interestingly, the ionospheric flow enhancements reported in **Paper IV** had several properties in common with ionospheric Travelling Convection Vortices (TCVs) and the related Magnetic Impulse Events (MIEs) [Kataoka et al., 2001, 2003]. In particular, statistical studies [e.g., Sibeck and Korotova, 1996; Kataoka et al., 2003] show that the MIE/TCV occurrence has a preference for radial IMF orientation.

Chapter 5

Conclusions and Outlook

In this thesis we have investigated the dynamic surroundings of space plasma shocks: parallel and perpendicular geometries and their interplay; particle acceleration in a system involving them both; foreshock region on the upstream side and magnetosheath region on the downstream side. The key method has been the utilization of multi-point, multi-instrument observations to form a coherent interpretation of the event and a deeper understanding of the physics.

Paper I and **Paper II** addressed particle acceleration in shock–shock interaction—a fundamental acceleration mechanism that often takes place in astrophysical environments but that is very rarely seen *in situ*. The search for an explanation of the peculiar energetic particle observations at Geotail led us to a detailed analysis of a shock–shock interaction event with the best spacecraft coverage reported so far. The novel result was the first *in situ* observations of the particle release at shock collision, further verified with a simulation study.

In **Paper III** we investigated a class of transient phenomena in the magnetosheath: Earthward directed jets with a high speed unexpected for the subsolar region. Based on the detailed multi-spacecraft observations by Cluster we proposed a formation mechanism for the jets whose source had remained unexplained. We inferred a connection between the rippling of shock fronts evident in many observations and simulations and the structuring of the downstream region. The mechanism provides a mesoscale description for a process that is inherently connected to the kinetic scale interactions in the foreshock.

In the following study of **Paper IV** on the properties of several jets we found that they agree well with the proposed mechanism. We further investigated the possible role of the high dynamic pressure jets in the solar

wind–magnetosphere interaction and found that their effects could be seen in the magnetosphere all the way to the ground magnetometers.

In the immediate future it easy to see improvements to the numerical model we used in **Paper II**: a fully three-dimensional version, MHD background fields, and scattering using wave-observation-based mean free paths. The model was indeed able to reproduce the main features of the observed profiles and enforce the particle release scenario, but the final peak flux was not as high as observed. Implementation of scattering could remedy this, and also allow comparison with Interball observations deep in the foreshock. Scattering would probably also be a necessary ingredient in a model addressing shock–shock interaction at larger scales (e.g., ICME–CIR interaction or CME–CME interaction), where the magnetic connection between the shocks can be maintained for a longer time.

According to the Interball measurements, the enhanced particle acceleration resulted in a severe decrease in the foreshock magnetic pressure. As interplanetary shocks frequently impinge on the bow shock, a statistical study could be conducted to see how often such a diamagnetic cavity forms, how deep, and how it affects the IP shock propagation. On a more general level, the recent and possible future missions with imaging instruments, such as IBEX [McComas et al., 2009] and AXIOM [Sembay et al., 2012, and the references therein], provide intriguing possibilities for the study of IP shock–bow shock interactions.

Since the proposition of the formation mechanism in **Paper III**, the interest in magnetosheath jets has considerably increased. Other triggers have been proposed, but the local structure of the quasi-parallel shock plays a role in all of them. It would seem likely that although rotational discontinuities trigger formation of dynamic pressure fronts, the local rippling of the quasi-parallel bow shock breaks the fronts into smaller pulses. For steady radial IMF conditions, the rippling is probably sufficient by itself.

Clearly the future studies on the jets and their relation to other dayside transients (HFAs, foreshock bubbles, etc.) require a statistical approach. In the four years (2008–2011) of THEMIS data, 126 high speed jets with $P_{\mathrm{dyn}} \geq 1.5\, P_{\mathrm{dyn}}^{\mathrm{SW}}$ can be identified within the subsolar magnetosheath [Ferdinand Plaschke, personal communication]. The set of jets shows a strong preference for small IMF cone-angles. Further analysis of this data set will provide valuable information not only on the jets themselves but also on the solar wind conditions favourable for the their formation. Combined with magnetospheric and ground-based observations, the connection to MIEs/TCVs suggested in **Paper IV** can be studied as well.

Bibliography

[01]: Canadian Space Science Data Portal
`https://cssdp.ca`
cited on 8-Mar-2012.

[02]: Cluster Active Archive
`http://caa.estec.esa.int/caa/`
cited on 8-Mar-2012.

[03]: Coordinated Data Analysis Web
`http://cdaweb.gsfc.nasa.gov/`
cited on 8-Mar-2012.

[04]: Data ARchives and Transmission System (DARTS)
`http://darts.jaxa.jp`
cited on 8-Mar-2012.

[05]: Interball spacecraft
`http://www.iki.rssi.ru/interball/`
cited on 8-Mar-2012.

[06]: Interplanetary Monitoring Platform (IMP) 8 spacecraft
`http://spdf.gsfc.nasa.gov/imp8/project.html`
cited on 8-Mar-2012.

[07]: Solar Probe Plus mission
`http://solarprobe.gsfc.nasa.gov`
cited on 15-May-2012.

Acuña, M. H., Ogilvie, K. W., Baker, D. N., Curtis, S. A., Fairfield, D. H., and Mish, W. H.: The Global Geospace Science Program and Its Investigations, Space Sci. Rev., 71, 5–21, 1995.

Amata, E., Savin, S. P., Ambrosino, D., Bogdanova, Y. V., Marcucci, M. F., Romanov, S., and Skalsky, A.: High kinetic energy density jets in the

Earth's magnetosheath: A case study, Planet. Space Sci., 59, 482–494, 2011.

Archer, M., Horbury, T. S., and Eastwood, J. P.: Magnetosheath pressure pulses: Generation downstream of the bow shock from solar wind discontinuities, J. Geophys. Res., p. in press, 2012.

Bale, S. D., Mozer, F. S., and Horbury, T. S.: Density-Transition Scale at Quasiperpendicular Collisionless Shocks, Phys. Rev. Lett., 91, 265 004, 2003.

Bale, S. D., Balikhin, M. A., Horbury, T. S., Krasnoselskikh, V. V., Kucharek, H., Möbius, E., Walker, S. N., Balogh, A., Burgess, D., Lembège, B., Lucek, E. A., Scholer, M., Schwartz, S. J., , and Thomsen, M. F.: Quasi-perpendicular Shock Structure and Processes, Space Sci. Rev., 118, 161–203, 2005.

Balogh, A., Carr, C. M., Acuña, M. H., Dunlop, M. W., Beek, T. J., Brown, P., Fornaçon, K.-H., Georgescu, E., Glassmeier, K.-H., Harris, J., Musmann, G., Oddy, T., and Schwingenschuh, K.: The Cluster Magnetic Field Investigation: overview of in-flight performance and initial results, Ann. Geophys., 19, 1207–1217, 2001.

Balogh, A., Schwartz, S. J., Bale, S. D., Balikhin, M. A., Burgess, D., Horbury, T. S., Krasnoselskikh, V. V., Kucharek, H., Lembège, B., Lucek, E. A., Möbius, E., Scholer, M., Thomsen, M. F., and Walker, S. N.: Cluster at the Bow Shock: Introduction, Space Sci. Rev., 118, 155–160, 2005.

Blanco-Cano, X., Omidi, N., and Russell, C. T.: Macrostructure of collisionless bow shocks: 2. ULF waves in the foreshock and magnetosheath, J. Geophys. Res., 111, A10 205, 2006.

Blanco-Cano, X., Omidi, N., and Russell, C. T.: Global hybrid simulations: Foreshock waves and cavitons under radial interplanetary magnetic field geometry, J. Geophys. Res., 114, A01 216, 2009.

Blanco-Cano, X., Kajdic, P., Aguilar-Rodriguez, E., Russel, C. T., Jian, L., and Luhmann, J. G.: Interplanetary Shocks and Foreshocks observed by STEREO, abstract SH21B-1927 presented at 2011 Fall Meeting, AGU, San Francisco, Calif., 5–9 Dec, 2011.

Boyd, T. J. M. and Sanderson, J. J.: The Physics of Plasmas, Cambridge University Press, Cambridge, UK, 2003.

Burgess, D.: Foreshock-sshock interaction at collisionless quasi-parallel shocks, Adv. Space Res., 15, 159–169, 1995.

Burgess, D.: Particle Acceleration at the Earth's Bow Shock, Lect. Notes Phys., 725, 161–190, 2007.

Burgess, D., Lucek, E. A., Scholer, M., Bale, S. D., Balikhin, M. A., Balogh, A., Horbury, T. S., Krasnoselskikh, V. V., Kucharek, H., Lembège, B., Mobius, E., Schwartz, S. J., Thomsen, M. F., and Walker, S. N.: Quasi-parallel Shock Structure and Processes, Space Sc. Rev., 118, 205–222, 2005.

Cargill, P. J.: The interaction of collisionless shocks in astrophysical plasmas, Astrophys. J., 376, 771–781, 1991.

Cargill, P. J., Goodrich, C. C., and Papadopoulos, K.: Interaction of two collisionless shocks, Phys. Rev. Lett., 56, 1988–1991, 1986.

Chisham, G., Lester, M., Milan, S. E., Freeman, M. P., Bristow, W. A., Grocott, A., McWilliams, K. A., Ruohoniemi, J. M., Yeoman, T. K., Dyson, P. L., Greenwald, R. A., Kikuchi, T., Pinnock, M., Rash, J. P. S., Sato, N., Sofko, G. J., Villain, J.-P., and Walker, A. D. M.: A decade of the Super Dual Auroral Radar Network (SuperDARN): Scientific achievements, new techniques and future directions, Surv. Geophys., 28, 33–109, 2007.

Choudhuri, A. R.: The Physics of Fluids and Plasmas: An Introduction for Astrophysicists, Cambridge University Press, Cambridge, UK, 1998.

Classen, H.-T. and Mann, G.: Motion of ions reflected off quasi-parallel shock waves in the presence of large-amplitude magnetic field fluctuations, Astron. Astrophys., 330, 381–388, 1998.

Desai, M. I., Dayeh, M. A., Smith, C. W., Lee, M. A., and Mason, G. M.: Ion Acceleration Near CME-Driven Interplanetary Shocks, in: 32^{nd} International Cosmic Ray Conference, vol. 10, p. 53, 2011.

Dudkin, G. N., Lukanin, A. A., Nechaev, B. A., Peshkov, A. V., and Ryzhkov, V. A.: Observation of deuteron acceleration in a collision of magnetosonic shock waves in a plasma, JETP Lett., 55, 721–724, 1992.

Dudkin, G. N., Egorov, V. Y., Nechaev, B. A., and Peshkov, A. V.: Mechanism for ion acceleration in a collision of magnetosonic shock waves, JETP Lett., 61, 633–637, 1995.

Dudkin, G. N., Nechaev, B. A., and Padalko, V. N.: Simulation of the Formation of Accelerating Structures and Ion Acceleration in the Collision of Magnetosonic Shock Waves, Plasma Phys. Rep., 26, 502–506, 2000.

Eastwood, J. P., Lucek, E. A., Mazelle, C., Meziane, K., Narita, Y., Pickett, J., , and Treumann, R. A.: The Foreshock, Space Sci. Rev., 118, 41–94, 2005.

Escoubet, C. P., Schmidt, R., and Goldstein, M. L.: Cluster - science and mission overview, Space Sci. Rev., 79, 11–32, 1997.

Facskó, G., Trotignon, J., Dandouras, I., Lucek, E., and Daly, P.: Study of hot flow anomalies using Cluster multi-spacecraft measurements, Adv. Space Res., 45, 541–552, 2010.

Fairfield, D. H., Baumjohann, W., Paschmann, G., Lühr, H., and Sibeck, D. G.: Upstream Pressure Variations Associated with the Bow Shock and their Effects on the Magnetosphere, J. Geophys. Res., 95, 3773–3786, 1990.

Fermi, E.: On the Origin of the Cosmic Radiation, Phys. Rev., 75, 1169–1174, 1949.

Fisk, L. A.: Journey into the Unknown Beyond, Science, 309, 2016–2017, 2005.

Ganse, U., Kilian, P., Spanier, F., and Vainio, R.: Nonlinear Wave Interactions as Emission Process of Type II Radio Bursts, Astrophys. J., 751, 145, 2012.

Giacalone, J.: Energetic particle transport, in: Heliophysics: Space Storms and Radiation: Causes and Effects, edited by Schrijver, C. J. and Siscoe, G. L., pp. 233–262, Cambridge University Press, Cambridge, UK, 2010.

Giacalone, J., Schwartz, S. J., and Burgess, D.: Observations of suprathermal ions in associations with SLAMS, Geophys. Res. Lett., 20, 149–152, 1993.

Gloeckler, G.: In-situ detection of energetic particles, in: Heliophysics: Space Storms and Radiation: Causes and Effects, edited by Schrijver, C. J. and Siscoe, G. L., pp. 43–77, Cambridge University Press, Cambridge, UK, 2010.

Gold, R. E., Krimigis, S. M., Hawkins, S. E., Haggerty, D. K., Lohr, D. A., Fiore, E., Armstrong, T. P., G., H., and Lanzerotti, L. J.: Electron, Proton, and Alpha Monitor on the Advanced Composition Explorer spacecraft, Space Sci. Rev., 86, 541–562, 1998.

Gómez-Herrero, R., Malandraki, O., Dresing, N., Kilpua, E., Heber, B., Klassen, A., Müller-Mellin, R., and Wimmer-Schweingruber, R. F.: Spatial and temporal variations of CIRs: Multi-point observations by STEREO, J. Atmos. Solar-Terr. Phys., 73, 551–565, 2011.

Gosling, J. T., Bame, S. J., Feldman, W. C., Paschmann, G., Sckopke, N., and Russel, C. T.: Suprathermal Ions Upstream From Interplanetary Shocks, J. Geophys. Res., 89, 5409–5418, 1984.

Greenwald, R. A., Baker, K. B., Dudeney, J. R., Pinnock, M., Jones, T. B., Thomas, E. C., Villain, J.-P., Cerisier, J.-C., Senior, C., Hanuise, C., Hunsucker, R. D., Sofko, G., Koehler, J., Nielsen, E., Pellinen, R., Walker, A. D. M., Sato, N., and Yamagishi, H.: DARN/SuperDARN, A global view of the dynamics of high-latitude convection, Space Sci. Rev., 71, 761–796, 1995.

Grubb, R. N.: The SMS/GOES space environment monitor subsystem, NOAA Tech. Memo., ERL SEL-42, 1975.

Hundhausen, A. J. and Gosling, J. T.: Solar Wind Structure at Large Heliospheric Distances: An Interpretation of Pioneer 10 Observations, J. Geophys. Res., 81, 1436–1440, 1976.

Jacobsen, K. S., Phan, T. D., Eastwood, J. P., Sibeck, D. G., Moen, J. I., Angelopoulos, V., McFadden, J. P., Engebretson, M. J., Provan, G., Larson, D., and Fornaçon, K.-H.: THEMIS observations of extreme magnetopause motion caused by hot flow anomaly, J. Geophys. Res., 114, A08 210, 2009.

Jokipii, J. R.: A shock for Voyager 2, Nature, 454, 38–39, 2008.

Kataoka, R., Fukunishi, H., Lanzerotti, L. J., Maclennan, C. G., Frey, H. U., Mende, S. B., Doolittle, J. H., Rosenberg, T. J., and Weatherwax, A. T.: Magnetic impulse event: A detailed case study of extended ground and space observations, J. Geophys. Res., 106, 25 873–25 890, 2001.

Kataoka, R., Fukunishi, H., and Lanzerotti, L. J.: Statistical identification of solar wind origins of magnetic impulse events, J. Geophys. Res., 108, 1436, 2003.

Kennel, C. F., Edmiston, J. P., Scarf, F. L., Coroniti, F. V., Russell, C. T., Smith, E. J., Tsurutani, B. T., Scudder, J. D., Feldman, W. C., Anderson, R. R., Mozer, F. S., and Temerin, M.: Structure of the November 12, 1978, Quasi-Parallel Interplanetary Shock, J. Geophys. Res., 89, 5436–5452, 1984a.

Kennel, C. F., Scarf, F. L., Coroniti, F. V., Russell, C. T., Wenzel, K., Sanderson, T. R., van Nes, P., Feldman, W. C., Parks, G. K., Smith, E. J., Tsurutani, B. T., Mozer, F. S., Temerin, M., Anderson, R. R., Scudder, J. D., and Scholer, M.: Plasma and energetic particle structure upstream of a quasi-parallel interplanetary shock, J. Geophys. Res., 89, 5419–5435, 1984b.

Kennel, C. F., Edmiston, J. P., and Hada, T.: A quarter century of collisionless shock research, in: Collisionless Shocks in the Heliosphere: A Tutorial Review, edited by Stone, R. G. and Tsurutani, B. T., vol. 34 of *Geophys. Monogr. Ser.*, pp. 1–36, AGU, Washington, DC, 1985.

Kis, A., Scholer, M., Klecker, B., Kucharek, H., Lucek, E. A., and Rème, H.: Scattering of field-aligned beam ions upstream of Earth's bow shock, Annales Geophysicae, 25, 785–799, 2007.

Kokubun, S., Yamamoto, T., Acuña, M. H., Hayashi, K., Shiokawa, K., and Kawano, H.: The GEOTAIL Magnetic Field Experiment, J. Geomagn. Geoelectr., 46, 7–21, 1994.

Koskinen, H. E. J.: Physics of Space Storms: From the Solar Surface to the Earth, Springer, Berlin Heidelberg, 2011.

Krauss-Varban, D.: Particle acceleration in shocks, in: Heliophysics: Space Storms and Radiation: Causes and Effects, edited by Schrijver, C. J. and Siscoe, G. L., pp. 209–231, Cambridge University Press, Cambridge, UK, 2010.

Krauss-Varban, D., Li, Y., and Luhmann, J. G.: Ion Acceleration at the Earth's Bow Shock and at Interplanetary Shocks: A Comparison, in: Particle Acceleration and Transport in the Heliosphere and Beyond, 7^{th} Annual Astrophysics Conference, edited by Li, G., Hu, Q., Verkhoglyadova, O., Zank, G. P., Lin, R. P., and Luhmann, J. G., pp. 307–313, AIP, 2008.

Lembege, B., Giacalone, J., Scholer, M., Hada, T., Hoshino, M., Krasnoselskikh, V., Kucharek, H., Savoini, P., and Terasawa, T.: Selected Problems in Collisionless-Shock Physics, Space Sci. Rev., 110, 161–226, 2004.

Lembège, B., Savoini, P., Hellinger, P., and Trávníček, P. M.: Nonstationarity of a two-dimensional perpendicular shock: Competing mechanisms, J. Geophys. Res., 114, A03217, 2009.

Lembège, B., Ma, Y., and Deng, X.: Collision of two supercritical quasi-parpendicular nonstationary collisionless shocks: full particle simulations, abstract SM51B-1790 presented at 2010 Fall Meeting, AGU, San Francisco, Calif., 13–17 Dec, 2010.

Lin, R. P., Anderson, K. A., Ashford, S., Carlson, C., Curtis, D., Ergun, R., Larson, D., McFadden, J., McCarthy, M., Parks, G. K., Rème, H., Bosqued, J. M., Coutelier, J., Cotin, F., D'Uston, C., Wenzel, K., Sanderson, T. R., Henrion, J., Ronnet, J. C., and Paschmann, G.: A three-dimensional plasma and energetic particle investigation for the Wind spacecraft , Space Sci. Rev., 71, 125–153, 1995.

Lin, Y.: Global-scale simulation of foreshock structures at the quasi-parallel bow shock, J. Geophys. Res., 108, 1390, 2003.

Lin, Y. and Wang, X. Y.: Three-dimensional global hybrid simulation of dayside dynamics associated with the quasi-parallel bow shock, J. Geophys. Res., 110, A12 216, 2005.

Lin, Y., Lee, L. C., , and Yan, M.: Generation of dynamic pressure pulses downstream of the bow shock by variations in the interplanetary magnetic field orientation, J. Geophys. Res., 101, 479–493, 1996a.

Lin, Y., Swift, D. W., , and Lee, L. C.: Simulation of pressure pulses in the bow shock and magnetosheath driven by variations in interplanetary magnetic field direction, J. Geophys. Res., 101, 27 251–27 269, 1996b.

Livesey, W. A., Russell, C. T., and Kennel, C. F.: A comparison of specularly reflected gyrating ion orbits with observed shock foot thicknesses, J. Geophys. Res., 89, 6824–6828, 1983.

Lucek, E. A., Horbury, T. S., Dunlop, M. W., Cargill, P. J., Schwartz, S. J., Balogh, A., Brown, P., Carr, C., Fornacon, K. H., and Georgescu, E.: Cluster magnetic field observations at a quasi-parallel bow shock, Ann. Geophys., 20, 1699–1710, 2002.

Lucek, E. A., Horbury, T. S., Balogh, A., Dandouras, I., , and Rème, H.: Cluster observations of structures at quasi-parallel bow shocks, Ann. Geophys., 22, 2309–2314, 2004.

Lucek, E. A., Constantinescu, D., Goldstein, M. L., Pickett, J., Pinçon, J. L., Sahraoui, F., Treumann, R. A., and Walker, S. N.: The Magnetosheath, Space Sci. Rev., 118, 95–152, 2005.

Lucek, E. A., Horbury, T. S., Dandouras, I., and Rème, H.: Cluster observations of the Earth's quasi-parallel bow shock, J. Geophys. Res., 113, A07S02, 2008.

Lugaz, N., Manchester IV, W. B., Roussev, I. I., and Gombosi, T. I.: Observational evidence of CMEs interacting in the inner heliosphere as inferred from MHD simulations, J. Atmos. Solar-Terr. Phys., 70, 598–604, 2008.

Mann, G., Lühr, H., and Baumjohann, W.: Statistical analysis of short large-amplitude magnetic field structures in the vicinity of the quasi-parallel bow shock, J. Geophys. Res., 99, 13 315–13 323, 1994.

McComas, D. J., Bame, S. J., Barker, P., Feldman, W. C., Phillips, J. L., Riley, P., and Griffee, J. W.: Solar Wind Electron Proton Alpha Monitor (SWEPAM) for the Advanced Composition Explorer, Space Sci. Rev., 86, 563–612, 1998.

McComas, D. J., Allegrini, F., Bochsler, P., Bzowski, M., Collier, M., Fahr, H., Fichtner, H., Frisch, P., Funsten, H. O., Fuselier, S. A., Gloeckler, G., Gruntman, M., Izmodenov, V., Knappenberger, P., Lee, M., Livi, S., Mitchell, D., Möbius, E., Moore, T., Pope, S., Reisenfeld, D., Roelof, E., Scherrer, J., Schwadron, N., Tyler, R., Wieser, M., Witte, M., Wurz, P., and Zank, G.: IBEX—Interstellar Boundary Explorer, Space Sci. Rev., 146, 11–33, 2009.

Merka, J., Szabo, A., Slavin, J. A., and Peredo, M.: Three-dimensional position and shape of the bow shock and their variation with upstream Mach numbers and interplanetary magnetic field orientation, J. Geophys. Res., 110, A04 202, 2005.

Meziane, K., Hull, A. J., Hamza, A. M., and Lin, R. P.: On the bow shock θ_{Bn} dependence of upstream 70 keV to 2 MeV ion fluxes, J. Geophys. Res., 107, 1243, 2002.

Nemecek, Z., Safrankova, J., Prech, L., Sibeck, D. G., Kokubun, S., and Mukai, T.: Transient flux enhancements in the magnetosheath, Geophys. Res. Lett., 25, 1273–1276, 1998.

Neugebauer, M. and Giacalone, J.: Multispacecraft observations of interplanetary shocks: Nonplanarity and energetic particles, J. Geophys. Res., 110, A12 106, 2005.

Neugebauer, M., Goldstein, R., and Goldstein, B. E.: Features observed in the trailing regions of interplanetary clouds from coronal mass ejections, J. Geophys. Res., 102, 19 743–19 751, 1997.

Nishida, A.: The Geotail Mission, Geophys. Res. Lett., 21, 2871–2873, 1994.

Ogilvie, K. W., Chornay, D. J., Fritzenreiter, R. J., Hunsaker, F., Keller, J., Lobell, J., Miller, G., Scudder, J. D., Sittler, Jr., E. C., Torbert, R. B., Bodet, D., Needell, G., Lazarus, A. J., Steinberg, J. T., Tappan, J. H., Mavretic, A., and Gergin, E.: SWE, A Comprehensive Plasma Instrument for the Wind Spacecraft, Space Sci. Rev., 71, 55–77, 1995.

Oh, S. Y., Yi, Y., and Kim, Y. H.: Solar Cycle Variation of the Interplanetary Forward Shock Drivers Observed at 1 AU, Solar Physics, 245, 391–410, 2007.

Omidi, N., Blanco-Cano, X., and Russell, C. T.: Macrostucture of collisionless bow shocks: 1. Scale lengths, J. Geophys. Res., 110, A12 212, 2005.

Omidi, N., Sibeck, D. G., and Blanco-Cano, X.: Foreshock compressional boundary, J. Geophys. Res., 114, A08 205, 2009.

Omidi, N., Eastwood, J. P., and Sibeck, D. G.: Foreshock bubbles and their global magnetospheric impacts, J. Geophys. Res., 115, A06 204, 2010.

Plaschke, F., Glassmeier, K.-H., Sibeck, D. G., Auster, H. U., Angelopoulos, O. D. C. V., and Magnes, W.: Magnetopause surface oscillation frequencies at different solar wind conditions, Ann. Geophys., 27, 4521–4532, 2009.

Pomoell, J., Vainio, R., and Kissmann, R.: MHD Modeling of Coronal Large-Amplitude Waves Related to CME Lift-off, Solar Physics, 253, 249–261, 2008.

Prech, L., Nemecek, Z., and Safrankova, J.: Influence of the foreshock of the Earth's bow shock on the interplanetary shock propagation during their mutual interaction, Earth Planets Space, 61, 607–610, 2009.

Reames, D. V.: Particle Acceleration at the Sun and in the Heliosphere, Space Sci. Rev., 90, 413–491, 1999.

Rème, H., Aoustin, C., Bosqued, J. M., Dandouras, I., Lavraud, B., Sauvaud, J. A., Barthe, A., Bouyssou, J., Camus, T., Coeur-Joly, O.,

Cros, A., Cuvilo, J., Ducay, F., Garbarowitz, Y., Medale, J. L., Penou, E., Perrier, H., Romefort, D., Rouzaud, J., Vallat, C., Alcaydé, D., Jacquey, C., Mazelle, C., D'Uston, C., Möbius, E., Kistler, L. M., Crocker, K., Granoff, M., Mouikis, C., Popecki, M., Vosbury, M., Klecker, B., Hovestadt, D., Kucharek, H., Kuenneth, E., Paschmann, G., Scholer, M., Sckopke, N., Seidenschwang, E., Carlson, C. W., Curtis, D. W., Ingraham, C., Lin, R. P., McFadden, J. P., Parks, G. K., Phan, T., Formisano, V., Amata, E., Bavassano-Cattaneo, M. B., Baldetti, P., Bruno, R., Chionchio, G., di Lellis, A., Marcucci, M. F., Pallocchia, G., Korth, A., Daly, P. W., Graeve, B., Rosenbauer, H., Vasyliunas, V., McCarthy, M., Wilber, M., Eliasson, L., Lundin, R., Olsen, S., Shelley, E. G., Fuselier, S., Ghielmetti, A. G., Lennartsson, W., Escoubet, C. P., Balsiger, H., Friedel, R., Cao, J.-B., Kovrazhkin, R. A., Papamastorakis, I., Pellat, R., Scudder, J., and Sonnerup, B.: First multispacecraft ion measurements in and near the Earth's magnetosphere with the identical Cluster ion spectrometry (CIS) experiment, Ann. Geophys., 19, 1303–1354, 2001.

Russell, C. T., Mellott, M. M., Smith, E. J., and King, J. H.: Multiple spacecraft observations of interplanetary shocks: Four spacecraft determination of shock normals, J. Geophys. Res., 88, 4739–4748, 1983.

Russell, C. T., Petrinec, S. M., Zhang, T. L., Song, P., and Kawano, H.: The effect of foreshock on the motion of the dayside magnetopause, Geophys. Res. Lett., 24, 1439–1441, 1997.

Russell, C. T., Wang, Y. L., Raeder, J., Tokar, R. L., Smith, C. W., Ogilvie, K. W., Lazarus, A. J., Lepping, R. P., Szabo, A., Kawano, H., Mukai, T., Savin, S., Yermolaev, Y. I., Zhou, X.-Y., and Tsurutani, B. T.: The interplanetary shock of September 24, 1998: Arrival at Earth, J. Geophys. Res., 105, 25 143–25 154, 2000.

Russell, C. T., Jian, L. K., Cano, X. B., Luhmann, J. G., and Zhang, T. L.: STEREO observations of shock formation in the solar wind, Geophys. Res. Lett., 36, L02 103, 2009.

Safrankova, J., Zastenker, G., Nemecek, Z., Fedorov, A., Simersky, M., and Prech, L.: Small scale observation of magnetopause motion: preliminary results of the INTERBALL project, Ann. Geophys., 15, 562–569, 1997.

Sandroos, A. and Vainio, R.: Particle acceleration at shocks propagating in inhomogeous magnetic fields, A&A, 455, 685–695, 2006.

Sandroos, A. and Vainio, R.: Reacceleration fo flare ions in coronal and interplanetary shock waves, Ap. J. S., 181, 183–196, 2009.

Sanny, J., Tapia, J. A., Sibeck, D. G., and Moldwin, M. B.: Quiet-time variability of the geosynchronous magnetic field and its response to the solar wind, J. Geophys. Res., 107, 1443, 2002.

Savin, S., Amata, E., Zelenyi, L., Budaev, V., Treumann, R., Lucek, E., Safrankova, J., Nemezek, Z., Khotyaintsev, Y., Andre, M., Buechner, J., Alleyne, H., Song, P., Blecki, J., Rauch, J. L., Romanov, S., Klimov, S., and Skalsky, A.: High kinetic energy jets in the Earth's magnetosheath: Implications for plasma dynamics and anomalous transport, JETP Lett., 87, 593–599, 2008.

Savin, S., Budaev, V., Zelenyi, L., Amata, E., Sibeck, D., Lutsenko, V., Borodkova, N., Zhang, H., Angelopoulos, V., Safrankova, J., Nemecek, Z., Blecki, J., Buechner, J., Kozak, L., Romanov, S., Skalsky, A., and Krasnoselsky, V.: Anomalous Interaction of a Plasma Flow with the Boundary Layers of a Geomagnetic Trap, JETP Lett., 96, 754–762, 2011.

Savin, S., Amata, E., Zelenyi, L., Lutsenko, V., Safrankova, J., Nemecek, Z., Borodkova, N., Buechner, J., Daly, P. W., Kronberg, E. A., Blecki, J., Budaev, V., Kozak, L., Skalsky, A., and Lezhen, L.: Super fast plasma streams as drivers of transient and anomalous magnetospheric dynamics, Ann. Geophys., 30, 1–7, 2012.

Scholer, M. and Ipavich, F. M.: Energetic Ions Upstream of the Earth's Bow Shock During an Energetic Storm Particle Event, J. Geophys. Res., 88, 5715–5726, 1983.

Schwartz, S. J.: Magnetic field structures and related phenomena at quasi-parallel shocks, Adv. Space Res., 11, 231–240, 1991.

Schwartz, S. J.: Shock and Discontinuity Normals, Mach Numbers, and Related Parameters, in: Analysis Methods for Multi-Spacecraft Data, edited by Paschmann, G. and Daly, P. W., vol. 001 of *ISSI Sci. Reports*, pp. 249–270, ESA, Noordwijk, The Netherlands, 1998.

Schwartz, S. J.: Shocks: Commonalities in Solar-Terrestrial Chains, Space Sci. Rev., 124, 333–344, 2006.

Schwartz, S. J. and Burgess, D.: Quasi-parallel shocks: A patchwork of three-dimensional structures, Geophys. Res. Lett., 18, 373–376, 1991.

Schwartz, S. J., Henley, E., Mitchell, J., and Krasnoselskikh, V.: Electron Temperature Gradient Scale at Collisionless Shocks, Phys. Rev. Lett., 107, 215 002, 2011.

Sembay, S., Branduardi-Raymont, G., Eastwood, J., Sibeck, D., Abbey, A., Brown, P., Carter, J., Carr, C., Forsyth, C., Kataria, D., Kemble, S., Milan, S., Owen, C., Read, A., Peacocke, L., Arridge, C., Coates, A., Collier, M., Cowley, S., Fazakerley, A., Fraser, G., Jones, G., Lallement, R., Lester, M., Porter, F., and Yeoman, T.: AXIOM: Advanced X-ray imaging of the magnetosheath, Astron. Nachr., 333, 388–392, 2012.

Shue, J.-H., Chao, J.-K., Song, P., McFadden, J. P., A. Suvorova, 1 V. Angelopoulos, . K. H. G., , and Plaschke, F.: Anomalous magnetosheath flows and distorted subsolar magnetopause for radial interplanetary magnetic fields, Geophys. Res. Lett., 36, L18 112, 2009.

Sibeck, D. G. and Korotova, G. I.: Occurrence patterns for transient magnetic field signatures at high latitudes, J. Geophys. Res., 101, 13 413–13 428, 1996.

Sibeck, D. G., Baumjohann, W., Elphic, R. C., Fairfield, D. H., Fennell, J. F., Gail, W. B., Lanzerotti, L. J., Lopez, R. E., Luehr, H., Lui, A. T. Y., Maclennan, C. G., McEntire, R. W., Potemra, T. A., Rosenberg, T. J., and Takahashi, K.: The Magnetospheric Response to 8-Minute Period Strong-Amplitude Upstream Pressure Variations, J. Geophys. Res., 94, 2505–2519, 1989.

Sibeck, D. G., Omidi, N., Dandouras, I., and Lucek, E.: On the edge of the foreshock: model-data comparisons, Ann. Geophys., 26, 1539–1544, 2008.

Sonnerup, B. U. Ö. and Scheibles, M.: Minimum and Maximum Variance Analysis, in: Analysis Methods for Multi-Spacecraft Data, edited by Paschmann, G. and Daly, P. W., vol. 001 of *ISSI Sci. Reports*, pp. 185–220, ESA, Noordwijk, The Netherlands, 1998.

Stone, E. C., Frandsen, A. M., Mewaldt, R. A., Christian, E. R., Margolies, D., Ormes, J. F., and Snow, F.: The Advanced Composition Explorer, Space Sci. Rev., 86, 1–22, 1998.

Stone, R. G. and Tsurutani, B. T., eds.: Collisionless Shocks in the Heliosphere: A Tutorial Review, vol. 34 of *Geophys. Monogr. Ser.*, AGU, Washington, DC, 1985.

Suvorova, A. V., Shue, J.-H., Dmitriev, A. V., Sibeck, D. G., McFadden, J. P., Hasegawa, H., Ackerson, K., Jelínek, K., Šafránková, J., and Němeček, Z.: Magnetopause expansions for quasi-radial interplanetary magnetic field: THEMIS and Geotail observations, J. Geophys. Res., 115, A10 216, 2010.

Szabo, A.: Determination of interplanetary shock characteristics, in: Proc. Solar Wind 11 / SOHO 16, Connecting Sun and Heliosphere, edited by B. Fleck, T.H. Zurbuchen, H. L., vol. 592, p. 449, 2005.

Terasawa, T., Shimada, N., Tsuboubouchi, K., Hoshino, M., Mukai, T., Saito, Y., Yamamoto, T., Nishida, A., Machida, S., Kokubun, S., Matsumoto, H., Kojima, H., Sanderson, T. R., Lazarus, A. J., Steinberg, J. T., and Lepping, R. P.: Particle acceleration at the interplanetary shock ahead of a large magnetic cloud on October 18, 1995: GEOTAIL-WIND collaboration, Adv. Space Res., 20, 641–644, 1997.

Treumann, R. A.: Fundamentals of collisionless shocks for astrophysical application, 1. Non-relativistic shocks, Astron. Astrophys. Rev., 17, 409–535, 2009.

Turner, D. L., Eriksson, S., Phan, T. D., Angelopoulos, V., Tu, W., Liu, W., Li, X., Teh, W., McFadden, J. P., and Glassmeier, K.: Multispacecraft observations of a foreshock-induced magnetopause disturbance exhibiting distinct plasma flows and an intense density compression, J. Geophys. Res., 116, A04 230, 2011a.

Turner, D. L., Omidi, N., Sibeck, D. G., and Angelopoulos, V.: First observations of a foreshock bubble: implications for global magnetospheric dynamics and particle acceleration, abstract SM52B-02 presented at 2011 Fall Meeting, AGU, San Francisco, Calif., 5–9 Dec, 2011b.

Umeda, T., Kidani, Y., Matsukiyo, S., and Yamazaki, R.: Modified two-stream instability at perpendicular collisionless shocks: Full particle simulations, J. Geophys. Res., 117, A03 206, 2012.

Vainio, R., Kocharov, L., and Laitinen, T.: Interplanetary and Interacting Protons Accelerated in a Parallel Shock Wave, Astrophys. J., 528, 1015–1025, 2000.

Washimi, H., Zank, G. P., Hu, Q., Tanaka, T., and Munakata, K.: A Forecast of the Heliospheric Termination-Shock Position by Three-dimensional MHD Simulations, Astrophys. J. Lett., 670, L139, 2007.

Watermann, J., Vainio, R., Lilensten, J., Belehaki, A., and Messerotti, M.: The State of Space Weather Scientific Modeling—An Introduction, Space Sci. Rev., 147, 111–120, 2009.

Webb, G. M., Axford, W. I., and Terasawa, T.: On the drift mechanism for energetic charged particles at shocks, Astrophys. J., 270, 537–553, 1983.

Wilkinson, W. P.: The Earth's quasi-parallel bow shock: Review of observations and perspectives for Cluster, Planet. Space Sci., 51, 629–647, 2003.

Williams, D. J., McEntire, R. W., Schlemm, C. I., Lui, A. T. Y., Gloeckler, G., Christon, S. P., and Gliem, F.: GEOTAIL energetic particles and ion composition instrument, J. Geomagn. Geoelectr., 46, 39–57, 1994.

Yang, Z. W., Lu, Q. M., Lembège, B., and Wang, S.: Shock front nonstationarity and ion acceleration in supercritical perpendicular shocks, J. Geophys. Res., 114, A03 111, 2009.

Zhang, H., Sibeck, D. G., Omidi, N., Zong, Q., McFadden, J. P., Larson, D. E., Glassmeier, K., and Angelopoulos, V.: Hot Flow Anomalies & Foreshock Cavities – Are They the Same Thing?, abstract SM52B-01 presented at 2011 Fall Meeting, AGU, San Francisco, Calif., 5–9 Dec, 2011.